Clearance of genome-damaged cells from the hematopoietic system via p53 without contribution by the cGAS/STING axis

Nicole Dressel[1]*, Loreen Natusch[1]*, Clara M. Munz[1], Santiago Costas[1], Mina N.F. Morcos[1], Anja Hoppe[1], Björn Hiller[1], Hella Luksch[2], Angela Rösen-Wolff[2], Axel Roers[1#], Rayk Behrendt[1#], Alexander Gerbaulet[1#]

[1]Institute for Immunology, Medical Faculty TU Dresden
[2]Department of Pediatrics, University Hospital Carl Gustav Carus, TU Dresden
* equal contribution, # senior author

correspondence: alexander.gerbaulet@tu-dresden

Abstract

Cell-intrinsic response patterns control risks arising from genome-damaged cells, preventing malignant transformation. p53-dependent DNA damage responses halt the cell cycle and induce either repair, senescence or cell death. Cyclic-GMP-AMP synthase (cGAS) has emerged as a new principle detecting genome damage and activating complex response programs. This DNA sensor is activated by micronuclei, chromosome bridges and prolonged mitotic arrest. STING-responses downstream of cGAS can drive cells into senescence or cell death through the induction of antiproliferative type I interferons (IFN) and proapoptotic tumor necrosis factor. Herein, we investigated how DNA damage-dependent and DNA-damage independent chronic activation of cGAS/STING signaling impacts on hematopoiesis. Hematopoietic loss of ribonucleotide excision repair (RER) resulted in chromosomal instability and activation of the cGAS/STING/IFN axis. Mice with hematopoietic RER-deficiency displayed compromised hematopoietic stem cell (HSC) function resulting in cytopenia and ultimately developed leukemia. Additional loss of p53 largely rescued mature blood cell production at the cost of accelerated leukemogenesis, while concurrent loss of cGAS, STING or type I IFN signalling had no detectable effect on HSC function, cytopenia and leukemia development in RER-deficient hematopoiesis. Also in models of acute genome damage, cGAS was irrelevant for the initial cell loss as well as the subsequent recovery of hematopoiesis. In contrast, a constitutive STING gain-of-function mutation impaired HSC functions independently of DNA damage. Collectively, we present *in vivo* evidence that the cGAS/STING pathway does not influence the capacity of the hematopoietic system to cope with DNA damage. Nevertheless, chronic activation of STING dramatically reduced the fitness of HSCs. (251 words)

Introduction

Genome integrity is continuously challenged by damage to genomic DNA resulting from spontaneous hydrolysis of phosphodiester bonds, ionizing radiation, mutagenic chemicals or reactive oxygen species

(Lindahl 2016). Cells detect DNA damage and activate signaling cascades to halt the cell cycle and induce repair pathways (Jackson and Bartek 2009). The tumor suppressor p53 is key in cellular responses to diverse forms of stress, including genome damage. DNA damage signaling stabilizes p53 protein, allowing it to regulate transcription of a plethora of genes. Depending on quality of DNA damage, signal intensity and cell type, p53 mediates cell cycle arrest, triggers DNA repair, activates different forms of programmed cell death or drives cells into senescence (Vousden and Prives 2009, Ou and Schumacher 2018, Hafner, Bulyk et al. 2019). Persistent DNA damage that cannot be repaired has fundamentally different consequences on short lived, post-mitotic cells, in contrast to long-lived cells with high proliferative potential like e.g. progenitor or even stem cells (Mandal, Blanpain et al. 2011).

Genome damage was recently demonstrated to activate cell-intrinsic type I interferon (IFN) production (Hartlova, Erttmann et al. 2015, Erdal, Haider et al. 2017, Mackenzie, Carroll et al. 2017, Hiller, Hoppe et al. 2018, Li and Chen 2018). An important link between genome damage and innate antiviral immunity is the pattern recognition receptor cyclic GMP-AMP synthase (cGAS), which detects double-stranded DNA. Upon ligation by DNA, cGAS catalyzes formation of a cyclic dinucleotide second messenger, cyclic guanosine monophosphate–adenosine monophosphate (cGAMP) that in turn activates the sensor stimulator of interferon genes (STING) to induce type I IFN and proinflammatory cytokine production. cGAS/STING responses are key to defend against DNA virus infections, but cGAS also recognizes endogenous DNA and can thereby contribute to various stress responses (Hopfner and Hornung 2020). Genome damage can yield two kinds of endogenous cGAS ligands. Damage resulting in chromosomal aberrations leads to problems of mitotic chromosome segregation and formation of micronuclei. Micronuclear chromatin can be sensed by cGAS and induce type I IFN (Mackenzie, Carroll et al. 2017). Moreover, enhanced DNA repair in genome-damaged cells can release oligonucleotide waste that leaks into the cytosol where it overwhelms degradation capacity of the cytosolic DNase TREX1, forms immunostimulatory cGAS ligands and activates IFN responses (Ahn, Xia et al. 2014, Shen, Le Bert et al. 2015, Erdal, Haider et al. 2017, Vanpouille-Box, Alard et al. 2017, Takahashi, Loo et al. 2018, Schubert, Schumann et al. 2022).

cGAS/STING signaling activated by genome damage induces type I IFN production. While stimulating proliferation of hematopoietic stem cells (HSCs) (Essers, Offner et al. 2009, Pietras, Lakshminarasimhan et al. 2014), type I IFN exerts robust antiproliferative effects on several types of more mature cells (Bromberg, Horvath et al. 1996, Sangfelt, Erickson et al. 2000, McNab, Mayer-Barber et al. 2015). In addition, cGAS/STING signaling can also trigger senescence and cell death (Gulen, Koch et al. 2017, Li and Chen 2018, Paludan, Reinert et al. 2019). Collectively, induction of antiproliferative type I IFN, senescence and cell death implicate the cGAS/STING axis as an important safeguard mechanism eliminating genome-damaged cells and thereby preventing cancer (Li and Chen 2018).

Herein, we address the effects of DNA damage and damage-induced cGAS/STING responses *in vivo*. We use mice deficient for RNase H2 (RH2) as a model for chronic DNA damage. RH2 is essential for the ribonucleotide excision repair (RER) pathway responsible for removal of the vast numbers of single ribonucleotides that the replicative polymerases misincorporate into genomic DNA during each S phase. Failure to repair these lesions results in genome instability, micronucleus formation, chronic activation of cGAS/STING and type I IFN production (Reijns, Rabe et al. 2012, Mackenzie, Carroll et al. 2016, Bartsch, Knittler et al. 2017, Mackenzie, Carroll et al. 2017, Hiller, Hoppe et al. 2018). We inactivated RH2 selectively in the entire hematopoietic system, avoiding the embryonic lethality associated with global deficiency for RNase H2 (Hiller, Achleitner et al. 2012). We find that the genome damage ensuing from loss of RER massively compromises hematopoiesis and results in malignant transformation. At the cost of accelerated leukemogenesis, blood cell production is largely rescued by additional loss of p53. Unexpectedly, inactivation of the cGAS/STING axis or of type I IFN signaling had no detectable impact on RER-deficient hematopoiesis. In addition, loss of cGAS/STING did neither alter steady state nor stress hematopoiesis. Our findings argue that the cGAS/STING axis does not significantly contribute to

protection of the hematopoietic system against DNA damage accumulation and malignant transformation.

Results

Hematopoietic loss of RER results in genome instability and predisposes to leukemia.

In order to investigate defense-mechanisms against genome damage in the hematopoietic system, we generated mice with loss of RER throughout hematopoiesis by conditional inactivation of the *Rnaseh2b* gene (Stadtfeld and Graf 2005, Hiller, Achleitner et al. 2012). As expected, *Rnaseh2b*$^{FL/FL}$ x Vav-Cre^{+} mice, ("RH2^{hKO}") featured high numbers of micronucleated erythrocytes (Figures 1A, B, S1E) reflecting genome instability ensuing from unrepaired ribonucleotides contained in the genomic DNA (Balmus, Karp et al. 2015, Kellner and Luke 2020). Except for a minor growth retardation (Figure S2A), the mutants are macroscopically indistinguishable from Cre-negative control littermates ("RH2^{hWT}") during the first 3 months of life. However, median survival was significantly reduced to about 13 months (Figure 1 C). Analysis of moribund mice at different age revealed a conspicuous enlargement of the thymus (Figures 1D, E). Histology showed a loss of normal thymic medulla and cortex architecture (Figure S2B) due to a massive expansion of CD4/8 double positive (DP) thymocytes (Figure 1F). In some of these animals, DP thymocytes disseminated to PB (Figure 1G) and spleen (Figure S2C), suggesting T cell acute lymphoblastic leukemia (T-ALL) like disease as the most likely cause of death in these animals. Some moribund mice did not show signs of leukemia as judged by macroscopic inspection of organs or immuno-phenotyping of PB, BM, thymus and spleen. These animals presented with very low hematocrit and leukocytes counts, suggesting hematopoietic failure or infection as the reason for lethality.

These data show that conditional inactivation of RER represents a suitable model for studies of bone marrow function under conditions of chronic DNA damage. In the following, we address blood cell generation of RH2^{hKO} mice in the balanced disease state before onset of malignancy.

High load of genome damage causes hematopoietic malfunction in RH2^{hKO} mice.

At young age, RH2^{hKO} animals featured massive alterations of the hematopoietic system. These included macrocytic anemia, almost complete absence of B cells, reduced T cell and granulocyte numbers, but elevated platelet counts (Figure 2A). Flow cytometric analysis of RH2^{hKO} bone marrow (BM) revealed that total cellularity was reduced to about one third of control BM. To robustly identify hematopoietic stem cells (HSCs, lineage^{-}EPCR^{+}Kit^{+} (LEK) CD48$^{-/lo}$CD150^{+}, Figure S1A) we substituted Sca-1, which was previously reported to be upregulated by type I IFN signaling (Essers, Offner et al. 2009, Kanayama, Izumi et al. 2020), by EPCR (CD201) (Figure 2B)(Vazquez, Inlay et al. 2015). Like HSCs, also absolute numbers of progenitor populations (see Figure S1A for gating) were massively reduced in RH2^{hKO} BM (Figure 2B). All populations of B-lymphocyte development from pre-pro B cells to mature B cells (see Figure S1B for gating) were reduced to below 10% of normal numbers (Figure 2C). Likewise, the thymi of RH2^{hKO} mice were severely reduced in weight (Figures S3A, B) and cellularity was only about 5% of controls (Figure 2D). Thymocytes of the first stages of T lymphocyte development (CD4/8 double-negative (DN) 1-3), see Figure S1C for gating) were reduced to about half of normal numbers and cells of later stages were almost completely absent (Figure 2D). About 10% of the RH2^{hKO} mice distinctly differed from the majority by ameliorated cytopenia (Figures S3D-G) and showed almost normal numbers of micronucleated erythrocytes (Figure S3H), but retained high Sca-1 expression (Figure S3I), most likely reflecting overgrowth of clones that had escaped Cre-mediated inactivation of *Rnaseh2b*.

To address stem cell fitness, we cultivated single HSCs and found a reduced proliferative capacity of RH2^{hKO} HSCs (Figures 2E, F). Moreover, we determined the functional potential of HSCs *in vivo* by competitive transplantation into lethally irradiated recipients and found a severe repopulation defect of RNaseH2-deficient HSCs (Figures 2G-I, S2J-K).

Taken together, chronic genome damage in the hematopoietic system of RH2^{hKO} mice reduced numbers, proliferation and repopulation capacity of HSCs. Impaired hematopoiesis resulted in anemia, lymphopenia and reduced granulocyte numbers.

Genome damage in RH2^{hKO} mice activates p53 and type I IFN signaling.

In order to elucidate how chronic genome damage leads to hematopoietic malfunction in RH2^{hKO} mice, we sorted myeloid progenitors (granulocyte-monocyte progenitors (GMP)) from BM of mutant and control animals (Figure S1A) and sequenced their transcriptome. We found 198 genes significantly up-regulated in RH2^{hKO} compared to control cells (Figure 3A, Table S1). Among the most upregulated genes were the ISGs *Oasl1*, *Mx1*, *Ifit1* (Figure 3B, Table S2) as well as *Cdkn1a*, encoding cell cycle inhibitor p21 and other p53-induded genes, including *Trp53inp1*, *Bax* and *Mdm2 (*Figure 3C, Table S3*)*. *Rnaseh2b* was the most downregulated gene, validating the analysis. In addition, *Ear1/2*, *Gzmb* and *Tspan9* were among 20 significantly downregulated genes. These results suggested induction of type I IFN and p53-mediated DNA damage responses in the mutant cells, which was confirmed by gene set enrichment analysis (GSEA, Figure 3D). We also found upregulation of several ISGs in bone marrow and spleen of RH2^{hKO} animals by qRT PCR (Figures S4A-C). Compatible with activation of a cGAS/STING response in RH2-deficient cells (Mackenzie, Carroll et al. 2017), GSEA also revealed induction of NF-κB-dependent proinflammatory gene expression in the mutant cells. In accordance with the ISG response on the transcriptome level, the type I IFN-induced surface protein Sca-1 was significantly upregulated on HSCs and PB lymphocytes from mutant compared to control mice as determined by flow cytometry (Figures 3E and S3C).

Attenuation of the p53 response rescues hematopoietic defects of RH2^{hKO} mice at the cost of accelerated leukemogenesis.

We next investigated the impact of the activated p53 response on the phenotype of RH2^{hKO} mice and crossed the animals to *Trp53*$^{KO/KO}$ mice (Donehower, Harvey et al. 1992). Heterozygous loss of *Trp53* significantly ameliorated the hematopoietic deficits caused by absence of RH2 activity (Figure 4A). Erythrocyte counts were significantly increased in RH2^{hKO}*Trp53*$^{KO/WT}$ mice compared to the severe anemia of RH2^{hKO} controls. PB B cells, virtually absent in RH2^{hKO} animals, reached about 2/3 of control numbers, while PB T cells numbers were back to normal. The conspicuous thrombocytosis of RH2^{hKO} mice was less pronounced. Whereas BM was still hypocellular, numbers of HSCs and progenitor populations were robustly increased in numbers compared to RH2^{hKO} BM, with MPPs and HPC-1 reaching control numbers (Figure 4B). Likewise, B cell and T cell development were partially rescued (Figures S5A, B).

Competitive transplantation revealed that the additional loss of one *Trp53* allele partially restored the repopulation deficit of RH2-deficient HSCs in primary (Figures 4 C-F) and secondary transplantation (Figures S5C-F). Heterozygous loss of p53 did not further increase the frequency of micronucleated erythrocytes in RH2-deficient hematopoiesis (Figure 4G). Lymphocytes (Figure 4H) and HSCs (Figure S5G) from RH2^{hKO}*Trp53*$^{KO/WT}$ mice still showed upregulation of the ISG Sca-1 compared to RH2^{hKO} controls.

While most parameters of RH2^{hKO} hematopoietic function were robustly improved by attenuated p53 expression, we observed a dramatically shortened median survival of RH2^{hKO}*Trp53*$^{KO/WT}$ animals in comparison to RH2^{hKO} animals (Figure 5A). In addition to development of T-ALL-like disease (Figure 1), some moribund RH2^{hKO}*Trp53*$^{KO/WT}$ animals featured grossly enlarged spleens with abnormal histology (Figures 5B, C). Flow cytometric analysis of BM, PB and spleen of these animals showed a massive expansion of aberrant lin^{-}CD117^{hi}Sca-1^{-}CD201^{-}CD34^{-}CD150^{-}CD48$^{-/lo}$ myeloid progenitor cells (Figures 5D, S6A), thus a condition resembling acute myeloid leukemia (AML). Some mice developed both, ALL- and AML-like disease simultaneously (Figure 5E), which was revealed by gross enlargement of thymus and spleen. Flow cytometric analysis uncovered DP thymocytes in peripheral blood and infiltration of CD117^{hi}Sca-1^{-} cells in the spleen (not shown). In addition, we generated few RH2^{hKO}p53$^{KO/KO}$ mice (n=4), which started to develop leukemic disease already by 8 weeks of age (Figure S6B-D). PB, BM and thymus

phenotyping of these animals revealed a more pronounced rescue of hematopoietic defects than in $RH2^{hKO}p53^{KO/WT}$ mice (Figures S6E-H), whilethe upregulation of Sca-1 persisted (Figure S6I)
In summary, attenuation of p53 signaling ameliorated the hematopoietic defects of $RH2^{hKO}$ animals, but simultaneously fueled leukemia development.

Signaling via the cGAS/STING axis has no impact on RER-deficient hematopoiesis.
Loss of RER in hematopoietic cells led to DNA damage, micronucleus formation, and activation of innate immune pathways and, ultimately, malignant transformation. As genome damage and micronuclear DNA had been shown to drive type I IFN via cGAS/STING in other models of RER deficiency (Mackenzie, Carroll et al. 2016, Mackenzie, Carroll et al. 2017), we crossed $RH2^{hKO}$ mice to $Cgas^{KO/KO}$, $Sting1^{GT/GT}$ or $Ifnar1^{KO/KO}$ animals. As expected, the enhanced expression of the type I IFN-induced surface protein Sca-1 in $RH2^{hKO}$ control mice was abrogated by each of these additional knock outs (Figure 6A), demonstrating that the cGAS/STING axis translated the genome damage of RER-defective hematopoietic cells into activation of type I IFN signaling.
Type I IFN exerts antiproliferative effects on numerous cell types (Bromberg, Horvath et al. 1996, Sangfelt, Erickson et al. 2000, McNab, Mayer-Barber et al. 2015), sensitizes to programmed cell death and is used to treat leukemic disease (Healy, Dahal et al. 2021). In addition to induction of type I IFN, STING activation was also shown to directly trigger cell death or senescence in a cell type and context-dependent manner (Gluck, Guey et al. 2017, Gulen, Koch et al. 2017, Li and Chen 2018, Paludan, Reinert et al. 2019). STING activation in $RH2^{hKO}$ mice could therefore be expected to contribute to suppression of hematopoiesis, elimination of damaged cells and prevention of leukemia. Unexpectedly, however, we detected no effect of defective cGAS/STING or IFNAR signaling on blood cell production in $RH2^{hKO}$ mice. All of the $RH2^{hKO}$ double KO mouse strains developed macrocytic anemia, leukopenia and thrombocytosis at young age, indistinguishable from RH2 single KO mice (Figures 6B-E, S7A). The repopulation defect of transplanted $RH2^{hKO}$ HSCs was not rescued by an additional loss of either cGAS or IFNAR (Figures 6F-I). Analysis of B lymphocyte and thymocyte development revealed persistent hematopoietic defects in $RH2^{hKO}Sting1^{GT/GT}$ mice (Figures S7B, C) Likewise, the proliferative potential of cultivated $RH2^{hKO}Sting1^{GT/GT}$ HSCs resembled that of $RH2^{hKO}$ HSCs (Figures 6J, K). Abrogation of cGAS/STING signaling in $RH2^{hKO}$ mice also had no effect on the frequency of micronucleated erythrocytes (Figures 6L, S7D). Collectively, in contrast to p53 signaling, the robust activation of cGAS/STING and type I IFN signaling of $RH2^{hKO}$ mice is not a relevant factor impairing hematopoiesis.
In accordance with these findings, neither cGAS/STING nor type I IFN signaling contributed to prevention of malignant disease as $RH2^{hKO}$ mice with an additional loss of either cGAS, STING or IFNAR exhibited a similar median survival as the $RH2^{hKO}$ animals (Figure 6M). Analysis of few moribund $RH2^{hKO}$ mice with additional loss of either cGAS, STING, or IFNAR revealed a similar pattern of leukemia (Figure 6N).
In summary, the cGAS/STING axis and type I IFN had no significant effect on the hematopoietic deficits or leukemogenesis of mice with severe genome damage throughout the hematopoietic system due to lack of RER.
Loss of cGAS does not alter steady state or stress hematopoiesis
Given that cGAS/STING signaling does not detectably impact on RER-deficient hematopoiesis, we next asked whether this pathway may be of relevance to control effects of spontaneous or acute DNA damage in wildtype mice. We first compared numbers of hematopoietic stem and progenitor cells as well as mature blood cells between $Cgas^{KO/KO}$ and WT control mice. As spontaneous background DNA damage accumulates with age, we investigated young and old animals. However, we found no differences in hematopoietic stem and progenitor cell numbers or mature blood cell counts in control versus $Cgas^{KO/KO}$ mice, neither young (Figure S8A-D) nor old (Figures S8 E, F). In order to address whether cGAS deficiency affects HSC proliferative capacity, we cultivated single HSCs purified from young and old $Cgas^{KO/KO}$ or $Cgas^{WT/WT}$ control mice and observed a similar growth pattern for both genotypes (Figures 7A, B & S7G,

H). HSC functionality was also unchanged *in vivo* as demonstrated by repopulation experiments. Serial competitive transplantation of HSC purified from young and old mice into lethally irradiated recipients did not reveal any effect of cGAS deficiency on HSC repopulation capacity (Figures 7C-F).

To address the relevance of cGAS-mediated responses to acute DNA damage, we investigated the recovery of the hematopoietic system from a single exposure to 2 Gy whole body γ-radiation. This acute genotoxic stress indeed resulted in cGAS/STING activation, as reflected in a sharp increase in expression of the type I IFN-induced surface protein Sca-1 that was largely blunted in the *Cgas*$^{KO/KO}$ animals (Figure 7G). As expected, irradiation caused a rapid loss of leukocytes, reticulocytes, and platelets (Figures 7H-J). After 5-10 days, white and red blood cell parameters started to recover, indicating compensatory mechanisms counteracting the radiation-induced blood cell loss. Neither the initial cell loss nor the following recovery phase was altered in *Cgas*$^{KO/KO}$ animals compared to control mice. Likewise, the numbers of surviving HSPCs, B- and T-lymphocyte progenitors (Figures S8I-L) after irradiation were not changed by lack of cGAS. Moreover, *in vitro*-proliferation of sorted HSCs irradiated with 2 Gy prior to cultivation was not altered by the absence of cGAS (Figures 7A, B S8G, H), and also repopulation potential of γ-irradiated HSCs, reduced compared to unirradiated HSCs as expected, was not affected by cGAS deficiency (Figures 7C-F). In addition to γ-irradiation, we also induced acute replication stress in cGAS-deficient and control mice by exposure to the myeloablative drug 5-fluorouracil (5-FU). This stressor causes rapid loss of cycling stem and progenitor cells and surviving cells subsequently initiate hematopoietic regeneration. However, loss of cGAS had no impact on the hematopoietic recovery after 5-FU-induced myeloablation (Figures 7 K-N, S8M-P).

A previous study (Jiang, Xue et al. 2019) reported that cGAS suppresses homologous recombination in a STING-independent fashion, and that loss of cGAS accordingly enhanced the resistance of hematopoietic cells to ionizing radiation. As we had not observed cGAS-mediated effects on the loss of hematopoietic cells upon whole body irradiation with 2Gy, we repeated this experiment with the same dose and observation intervals as in the study of Jiang et al. However, cGAS deficiency did not alter survival of hematopoietic stem and precursor cells or of mature blood cells 10 hours after 9 Gy whole body γ-irradiation (Figures 7O, P, S8Q)

In summary, loss of cGAS had no effect on steady-state hematopoiesis or stem cell function in young or old mice. cGAS appeared irrelevant for the survival or function of hematopoietic stem and progenitor cells upon exposure to acute genotoxic insults and accordingly for recovery of the hematopoietic system from genotoxic stress.

Chronic STING activation by SAVI-associated gain-of-function mutation massively impairs HSC potential

STING gain-of-function mutations cause "STING-associated vasculopathy with onset in infancy" (SAVI) (Liu, Jesus et al. 2014) and mouse models expressing homologous mutations have recently been generated and recapitulated important clinical and molecular features described in SAVI patients (Warner, Irizarry-Caro et al. 2017, Luksch, Stinson et al. 2019, Motwani, Pawaria et al. 2019). *Sting1*$^{N153S/WT}$ mice (Luksch, Stinson et al. 2019) feature overactive type I IFN and NFκB signaling, growth retardation and abnormal lymphocyte development, comparable to our observations in RH2^{hKO} mice, but lack significant DNA damage. Therefore, we used *Sting1*$^{N153S/WT}$ mice to study the effect of chronic STING activation on hematopoiesis in the absence of DNA damage. To circumvent pre-mature loss of HSC potential by continuous type I IFN activity (Essers, Offner et al. 2009), *Sting1*^{N153S} mice were maintained on an *Ifnar1*-deficient background. Single HSCs were purified from either *Sting1*$^{WT/WT}$*Ifnar1*$^{KO/KO}$ (WT) or *Sting1*$^{N153S/WT}$*Ifnar1*$^{KO/KO}$ (N153S) HSCs and cultured for ten days. After 96 hours of culture, an impaired proliferation of N153S HSC became evident and by day 10 of culture, colonies arising from single N153S HSCs were significantly smaller (Figures 8A, B). To examine the impact of constitutive STING activation on HSC potential *in vivo*, we competitively transplanted WT or N153S HSCs. (Figures 8C, D). The generation of B- and T-lymphocytes from N153S HSCs was severely impaired. Furthermore, we observed a mildly decreased contribution to PB neutrophils in primary recipients of N153S HSCs. In order to rigorously assess

long-term self-renewal of donor HSCs, we performed secondary transplantation and found a dramatically impaired contribution of N153S donor HSCs to all PB leukocytes including neutrophils. Final BM analysis of secondary recipients revealed loss of N153S donor HSCs. Taken together, our results in RH2 and *Sting1*^{N153S} mice support a model in which constitutive STING activation strongly impaired long-term self-renewal and transplantation potential of HSCs in a type I IFN and DNA damage-independent fashion.

Discussion

Here, we show that in a model of chronic genome damage causing massive cytopenia and cancer, in which both, p53 and cGAS/STING pathways are robustly activated, cGAS/STING appears irrelevant for hematopoietic function and prevention of malignant transformation. In contrast, p53 signaling eliminates large numbers of damaged cells, thereby causing cytopenia but efficiently delaying onset of leukemia. We also observed no cGAS/STING-mediated modulation of the impact of spontaneous or acute DNA damage on the hematopoietic system.

Major principles of detection of different forms of DNA damage and activation of appropriate repair have been elucidated over the past decades (Hoeijmakers 2009, Jackson and Bartek 2009, Ciccia and Elledge 2010). Sensor proteins of mismatch, base excision, nucleotide excision and ribonucleotide excision repair detect alterations of DNA and directly initiate local repair (Jiricny 2006, David, O'Shea et al. 2007, Hoeijmakers 2009, Williams, Lujan et al. 2016). Strand breaks are sensed by PI3 kinase-related enzymes, ATR, ATM and DNA-PK, which trigger the p53-mediated DNA damage response (Kastenhuber and Lowe 2017, Hafner, Bulyk et al. 2019). Depending on cell type and differentiation stage, as well as severity and persistence of the genomic lesions, this response halts the cell cycle and activates repair, or induces senescence or cell death to prevent malignant transformation (Hoeijmakers 2009, Jackson and Bartek 2009, Ciccia and Elledge 2010, Roos, Thomas et al. 2016). Recently, an additional principle alerting cells to genome damage and activating complex response programs emerged, the detection of double-stranded self-DNA (Hartlova, Erttmann et al. 2015, Erdal, Haider et al. 2017, Harding, Benci et al. 2017, Mackenzie, Carroll et al. 2017, Flynn, Koch et al. 2021). The presence of micronuclei or chromatin bridges reflects chromosomal instability and problems of mitotic segregation. Micronuclei and chromosome bridges activate the DNA sensor cGAS (Harding, Benci et al. 2017, Mackenzie, Carroll et al. 2017, Flynn, Koch et al. 2021). Likewise, prolonged mitotic arrest can lead to cGAS-mediated STING activation (Zierhut, Yamaguchi et al. 2019). Furthermore, acute genotoxic stress activates cGAS by release of DNA waste as a by-product of massive repair activity (Erdal, Haider et al. 2017). cGAS triggers STING activation to induce the antiviral type I IFNs, which mediate potent antiproliferative effects. STING also activates NF-kB and thereby links DNA damage to a second inflammatory pathway. Importantly, STING responses can also drive cells into senescence (Gluck, Guey et al. 2017, Yang, Wang et al. 2017) or cell death (Gaidt, Ebert et al. 2017, Gulen, Koch et al. 2017, Paludan, Reinert et al. 2019). These STING-mediated effector functions led to a view of STING as a contributor to control or elimination of severely genome damaged cells and prevention of cancer (Li and Chen 2018). How responses to damage mediated by p53 or STING relate to each other is unclear and differential relevance of both response patterns in different cell types or upon damage of different quality or intensity remains elusive.

Herein, we used deficiency for RER as an *in vivo* model of chronic DNA damage. Conditional inactivation of the *Rnaseh2b* gene selectively in the entire hematopoietic system resulted in viable mice that feature high numbers of micronucleated cells and progress to leukemia, reflecting genome damage and chromosomal instability. HSC function is compromised, B cells are almost completely absent, and T cells,

erythrocytes as well as myeloid cells are reduced, suggesting that DNA damage responses arrest or kill large numbers of genome-damaged cells. Transcriptome analysis revealed a signature of p53 target genes but also robust ISG and proinflammatory cytokine responses, suggesting STING activation, as had been seen in other cell types lacking RER (Hiller, Hoppe et al. 2018, Aden, Bartsch et al. 2019, Aditi, Downing et al. 2021). Inactivation of p53 significantly rescued HSC function and cytopenia, but resulted in accelerated leukemogenesis in mice with loss of RER in the hematopoietic system. In contrast, loss of cGAS or STING, which abrogated type I IFN and inflammatory cytokine responses, had no effect on blood cell production, survival or incidence of leukemia. Likewise, steady-state hematopoiesis was not detectably altered in the absence of cGAS or STING, indicating that this pathway is not required to control the impact of continuous low-level background DNA damage on hematopoiesis.

In mice with normal RH2 expression, inactivation of cGAS did not alter HSC function after acute genotoxic stress, in particular their capacity to repopulate lethally irradiated mice requiring massive proliferation. Moreover, the rapid death of vast numbers of cells upon sublethal whole body irradiation, as well as the subsequent recovery of blood cell production, were not detectably altered in mice lacking cGAS compared to WT littermates. The latter result was unexpected, as Jiang et al. had reported a STING-independent role of cGAS in suppression of homologous recombination repair of DNA-double strand breaks, sensitizing cells to programmed cells death after acute genotoxic stress (Jiang, Xue et al. 2019). To elucidate this discrepancy, we performed a precise repetition of the experiment by Jiang et al. and found massive cell death of HSPCs and mature hematopoietic cells in response to ionizing radiation in cGAS KO and WT animals.

Our findings put into perspective the role of cGAS/STING responses to DNA damage in hematopoietic cells *in vivo*. Neither cGAS nor STING are significant factors influencing the capacity of the hematopoietic system to cope with acute or chronic damage in the models investigated. The p53-mediated DNA damage response, on the other hand, eliminates vast numbers of damaged cells and efficiently delays malignant transformation, similar to earlier observations in mice lacking RH2 in epithelial lineages (Hiller, Hoppe et al. 2018, Aden, Bartsch et al. 2019). In line with our findings, a mouse model of RH2-deficiency in neuronal cells resulted in chronic genome damage and p53-dependent loss of cerebellar neurons without contribution by the cGAS/STING axis (Aditi, Downing et al. 2021).

RH2 KO mice developed thrombocythemia (Figure 2A), while all other blood lineages are cytopenic. These seemingly contradictory findings are likely explained by the observation that thrombocytes can be generated by direct differentiation of HSCs into megakaryocytes without proliferation (Morcos, Li et al. 2020), while maintenance of all other mature blood cells heavily relies on cell division of stem and progenitors cells. Interestingly, the thrombocythemia of $RH2^{hKO}$ mice was reversed by loss of p53, in line with reported roles for p53 signaling in megakaryocyte endoreplication and thrombopoiesis (Apostolidis, Woulfe et al. 2012, Yang, Liu et al. 2020).

While not relevant in the models of DNA damage investigated in our study, STING signaling in principle has the potential to massively impact on the hematopoietic system, as illustrated by the pronounced alterations of hematopoiesis caused by mutant, constitutively active STING in the human condition SAVI (Liu, Jesus et al. 2014)., which is characterized by myeloid cell expansions, but also severe lymphopenia. The inflammatory phenotype of these patients is reproduced in mouse models expressing gain-of-function mutations of STING (Warner, Irizarry-Caro et al. 2017, Luksch, Stinson et al. 2019, Motwani, Pawaria et al. 2019). We show that HSCs from such mice are functionally impaired. We speculate that

differential effects of STING activation by genome damage versus STING gain-of-function mutations are caused by differences of intensity, duration or quality of STING signaling. Moreover, embryonic and tissue stem cells were reported to be refractory to type I interferon signaling in order to protect these cells from over-activation, functional impairment and exhaustion (Wu, Dao Thi et al. 2018). However, constitutive STING-activation by the *Sting1*^{N153S} mutation resulted in loss of HSC function (Figure 8). Given that our transplantation experiment involved *Ifnar1*$^{KO/KO}$ HSCs, the functional impairment of *Sting1*$^{N153S/WT}$ HSCs must either be caused by cell-intrinsic STING effects or by NF-κB-driven proinflammatory cytokines.

Collectively, we show that STING responses have the potential to massively impact on hematopoietic cells production and differentiation and survival, but do not influence the capacity of the hematopoietic system to cope with acute or chronic DNA damage in the presence of functional p53. Future work will clarify whether cGAS/STING responses may represent a back-up surveillance pathway that becomes relevant upon loss of p53 function occurring frequently in malignant cells.

Acknowledgements

The authors thank Christa Haase, Livia Schulze and Madeleine Rickauer for expert technical assistance. This study was funded by the Fritz-Thyssen-Stiftung (Az. 10.19.1.013MN to A.G.), Deutsche Forschungsgemeinschaft (DFG, German Research Foundation) – Project-ID 369799452 – TRR237 Nucleic Acid Immunity, project B17 to A.R., project B19 to R.B. and project B18 to A.R.-W. L.N. was supported by the Elke-Kröner-Promotionskolleg.

Methods

Mice

The following mouse strain were used in the study*:* *Rnaseh2b*^{flox} (Hiller, Achleitner et al. 2012), Vav-Cre (Stadtfeld and Graf 2005)(kind gift from Claudia Waskow), *Ifnar1*^{KO} (Kamphuis, Junt et al. 2006), *Cgas*^{KO} (Schoggins, MacDuff et al. 2014), *Trp53*^{KO} (Donehower, Harvey et al. 1992), *Sting1*^{GT} (Sauer, Sotelo-Troha et al. 2011), *Sting1*^{N153S}(Luksch, Stinson et al. 2019). B6.CD45.1.
All animal experiments were in accordance with institutional guidelines and were approved by the relevant authority, Landesdirektion Dresden (TVV54/2017, TVV88/2017, TVV46/2019).

Cell Preparation

Bone marrow cells
Long bones (tibia, femora, pelvis) were crushed using mortar and pestle in PBS/2%FCS/2mM EDTA and filtered through a 100µm sieve. Erythrocytes were lysed by incubating in hypotonic NH4 Cl buffer for 5 min at room temperature. After washing, BM cells were filtered through a 30 µm mesh.
Thymocyte & splenocyte suspension
Either thymus or spleen were gently rubbed through 40µm cell strainer using PBS/2%FCS/2mM EDTA. After centrifugation, cells were subjected to erythrocyte lysis for 30, washed and filtered through a 30µm mesh.
Peripheral blood
Peripheral blood was drawn retro-orbitally into EDTA coated tubes (Sarstedt). PB was diluted 1:5 in isotonic saline and PB counts were determined on Sysmex XT2000i Vet hemacytometer. To obtain leukocyte suspension, PB was subjected to erythrocyte lysis two times for 5 min each and washed.

Absolute counts of all cell suspensions were determined employing a Miltenyi MACSquant analyzer.

Flow cytometry

Cell suspensions were incubated with pre-titrated monoclonal antibodies (see Table S4) for 30-40 min. After washing, cell suspensions were acquired on Miltenyi MACS 10 or BD LSR II analyzers or BD FACS ARIAII or ARIA III cell sorters. Flow cytometry data was analyzed using Flow Jo software version 9/10. Gates were set with help of fluorescence-minus-one controls

Bone marrow transplantation

BM cell suspension was depleted of lineage-positive cells using the mouse lineage cell depletion kit (Miltenyi) according to the manufacturer´s instructions. Lineage-negative BM cells were stained and immuno-phenotypic HSCs were sorted on BD FACS ARIAII & III cell sorters. Re-analysis revealed purity of sorted cells >95%. HSC were mixed with B6.CD45.1 whole bone marrow cells and retroorbitally injected into lethally-irradiated (9Gy, Xylon Maxishot X-ray tube) B6.CD45.1/CD45.2 recipients. For secondary transplantation, 5 x10^6 WBMCs were isolated from primary recipients and intravenously injected into lethally irradiated secondary recipients.

Micronuclei assay

Micronucleated erythrocytes were identified following the protocol of Balmus et al. (Balmus, Karp et al. 2015). Briefly, 30µl PB was mixed with 120µl PBS and fixed with pre-cooled (-80°C) methanol overnight and stored for maximum 1 year at -80%. Fixed erythrocytes were stained with antibodies against CD71 and Ter119 and digested 10µl RNase A (10mg/ml, Invitrogen) for 1hour at 4°C. Samples were washed and after adding 1µg/ml propidium iodide (PI), 1-2.5 x 10^6 events were acquired on a BD LSR II or BD FACS Aria III flow cytometer. Representative gating of micronucleated erythrocytes is shown in Figure S1E.

Single HSC culture

Single HSCs (LSK $CD48^{-/lo}CD150^{+}$ were deposited into 96 well round bottom plates (manufacturer). Single HSCs were cultivated for 10 days in Iscove´s modified Dulbecco´s medium (Gibco) supplemented with 20%FCS (Biochrom), Penicillin/Streptomycin, 20ng/ml rmSCF (Peprotech), 20 ng/ml rmTPO (Peprotech), rmIL-3 (Peprotech) and 5U/ml rhEPO (Janssen-Cilag). Cells were counted for the first 96h every 12h. After 10d, the total cell number of each single cell colony was determined on a Miltenyi MACSquant flow cytometer.

Histology

Thymus & spleen tissue was fixed overnight in 4% formalin fixative, followed by paraffin-embedding, sections were cut using a Leica microtome. Staining was performed according to H&E and May-Grüwald Giemsa protocol. Sections were analysed on a Keyence BZ-x710 microscope employing the 4x (Nikon Air PlanApo NA: 0,2 20mm) and 100x (Nikon Oil PlanApo NA:1,45 0,13mm) objectives.

RNA-seq

Lineage-negative BM cells were prepared from $RH2^{hKO}$ mice and $RH2^{hWT}$ littermate controls (n=4/genotype) and GMPs ($LE^{-}K$ $CD16/32^{hi}CD34^{+}$) were sorted. Total RNA was prepared using Qiagen RNeasy Micro kit.

Transcriptome analysis

Reads were mapped to mouse genome GRCm39 followed by normalization, exploratory and differential expression analysis using DESeq2 (Love, Huber et al. 2014). Unless otherwise stated, DEG lists were sorted according to ascending padj. All transcripts with padj<0.05 were subjected to GSEA (Subramanian, Tamayo et al. 2005). If not state otherwise, hallmark gene set collection (MSigDB) was used to identify enriched gene sets. To generate heatmaps all transcripts with padj<0.05 were extracted from lists containing normalized read counts of all genotypes in the respective experiment and the resulting sub list was displayed using Morpheus (https://software.broadinstitute.org/morpheus).

Quantitative PCR

Total RNA was isolated using NucleoSpin RNA Kit (Macherey-Nagel) and reverse transcribed into cDNA using PrimeScript RT Reagent Kit (Takara) following the manufacturer's instructions. Quantitative RT-PCR using Luna® Universal qPCR Master Mix (New England BioLabs) was performed with the following cycling conditions on a CFX384 Touch Real-Time PCR Detection System (Bio-Rad): 10 min 95°C, 40 cycles of 95°C for 20 s, 60°C for 30 s. The used qRT-PCR primers are listed in Supplementary Table S5. Transcript levels were normalized to the housekeeping gene Tbp1. All samples were run in technical triplicates.

Statistics

Statistical analysis was performed using Graphpad Prism 9, applied stastical tests are given in figure legends (ns= not significant, * = p <0.05 - 0.01, ** = p <0.01 – 0.001, *** = p < 0.001).

References

Aden, K., K. Bartsch, J. Dahl, M. A. M. Reijns, D. Esser, R. Sheibani-Tezerji, A. Sinha, F. Wottawa, G. Ito, N. Mishra, K. Knittler, A. Burkholder, L. Welz, J. van Es, F. Tran, S. Lipinski, N. Kakavand, C. Boeger, R. Lucius, W. von Schoenfels, C. Schafmayer, L. Lenk, A. Chalaris, H. Clevers, C. Rocken, C. Kaleta, S. Rose-John, S. Schreiber, T. Kunkel, B. Rabe and P. Rosenstiel (2019). "Epithelial RNase H2 Maintains Genome Integrity and Prevents Intestinal Tumorigenesis in Mice." Gastroenterology **156**(1): 145-159 e119.

Aditi, S. M. Downing, P. A. Schreiner, Y. D. Kwak, Y. Li, T. I. Shaw, H. R. Russell and P. J. McKinnon (2021). "Genome instability independent of type I interferon signaling drives neuropathology caused by impaired ribonucleotide excision repair." Neuron **109**(24): 3962-3979 e3966.

Ahn, J., T. Xia, H. Konno, K. Konno, P. Ruiz and G. N. Barber (2014). "Inflammation-driven carcinogenesis is mediated through STING." Nat Commun **5**: 5166.

Apostolidis, P. A., D. S. Woulfe, M. Chavez, W. M. Miller and E. T. Papoutsakis (2012). "Role of tumor suppressor p53 in megakaryopoiesis and platelet function." Exp Hematol **40**(2): 131-142 e134.

Balmus, G., N. A. Karp, B. L. Ng, S. P. Jackson, D. J. Adams and R. E. McIntyre (2015). "A high-throughput in vivo micronucleus assay for genome instability screening in mice." Nat Protoc **10**(1): 205-215.

Bartsch, K., K. Knittler, C. Borowski, S. Rudnik, M. Damme, K. Aden, M. E. Spehlmann, N. Frey, P. Saftig, A. Chalaris and B. Rabe (2017). "Absence of RNase H2 triggers generation of immunogenic micronuclei removed by autophagy." Hum Mol Genet **26**(20): 3960-3972.

Bromberg, J. F., C. M. Horvath, Z. Wen, R. D. Schreiber and J. E. Darnell, Jr. (1996). "Transcriptionally active Stat1 is required for the antiproliferative effects of both interferon alpha and interferon gamma." Proc Natl Acad Sci U S A **93**(15): 7673-7678.

Ciccia, A. and S. J. Elledge (2010). "The DNA damage response: making it safe to play with knives." Mol Cell **40**(2): 179-204.

David, S. S., V. L. O'Shea and S. Kundu (2007). "Base-excision repair of oxidative DNA damage." Nature **447**(7147): 941-950.

Donehower, L. A., M. Harvey, B. L. Slagle, M. J. McArthur, C. A. Montgomery, J. S. Butel and A. Bradley (1992). "Mice deficient for p53 are developmentally normal but susceptible to spontaneous tumours." Nature **356**: 215-221.

Erdal, E., S. Haider, J. Rehwinkel, A. L. Harris and P. J. McHugh (2017). "A prosurvival DNA damage-induced cytoplasmic interferon response is mediated by end resection factors and is limited by Trex1." Genes & Development **31**(4): 353-369.

Essers, M. A., S. Offner, W. E. Blanco-Bose, Z. Waibler, U. Kalinke, M. A. Duchosal and A. Trumpp (2009). "IFNalpha activates dormant haematopoietic stem cells in vivo." Nature **458**(7240): 904-908.

Flynn, P. J., P. D. Koch and T. J. Mitchison (2021). "Chromatin bridges, not micronuclei, activate cGAS after drug-induced mitotic errors in human cells." Proc Natl Acad Sci U S A **118**(48).

Gaidt, M. M., T. S. Ebert, D. Chauhan, K. Ramshorn, F. Pinci, S. Zuber, F. O'Duill, J. L. Schmid-Burgk, F. Hoss, R. Buhmann, G. Wittmann, E. Latz, M. Subklewe and V. Hornung (2017). "The DNA Inflammasome in Human Myeloid Cells Is Initiated by a STING-Cell Death Program Upstream of NLRP3." Cell **171**(5): 1110-1124 e1118.

Gluck, S., B. Guey, M. F. Gulen, K. Wolter, T. W. Kang, N. A. Schmacke, A. Bridgeman, J. Rehwinkel, L. Zender and A. Ablasser (2017). "Innate immune sensing of cytosolic chromatin fragments through cGAS promotes senescence." Nat Cell Biol **19**(9): 1061-1070.

Gulen, M. F., U. Koch, S. M. Haag, F. Schuler, L. Apetoh, A. Villunger, F. Radtke and A. Ablasser (2017). "Signalling strength determines proapoptotic functions of STING." Nat Commun **8**(1): 427.

Hafner, A., M. L. Bulyk, A. Jambhekar and G. Lahav (2019). "The multiple mechanisms that regulate p53 activity and cell fate." Nat Rev Mol Cell Biol **20**(4): 199-210.

Harding, S. M., J. L. Benci, J. Irianto, D. E. Discher, A. J. Minn and R. A. Greenberg (2017). "Mitotic progression following DNA damage enables pattern recognition within micronuclei." Nature **548**(7668): 466-470.

Hartlova, A., S. F. Erttmann, F. A. Raffi, A. M. Schmalz, U. Resch, S. Anugula, S. Lienenklaus, L. M. Nilsson, A. Kroger, J. A. Nilsson, T. Ek, S. Weiss and N. O. Gekara (2015). "DNA damage primes the type I interferon system via the cytosolic DNA sensor STING to promote anti-microbial innate immunity." Immunity **42**(2): 332-343.

Healy, F. M., L. N. Dahal, J. R. E. Jones, Y. Floisand and J. F. Woolley (2021). "Recent Progress in Interferon Therapy for Myeloid Malignancies." Front Oncol **11**: 769628.

Hiller, B., M. Achleitner, S. Glage, R. Naumann, R. Behrendt and A. Roers (2012). "Mammalian RNase H2 removes ribonucleotides from DNA to maintain genome integrity." The Journal of Experimental Medicine **209**(8): 1419-1426.

Hiller, B., A. Hoppe, C. Haase, C. Hiller, N. Schubert, W. Muller, M. A. M. Reijns, A. P. Jackson, T. A. Kunkel, J. Wenzel, R. Behrendt and A. Roers (2018). "Ribonucleotide Excision Repair Is Essential to Prevent Squamous Cell Carcinoma of the Skin." Cancer Res **78**(20): 5917-5926.

Hoeijmakers, J. H. (2009). "DNA damage, aging, and cancer." N Engl J Med **361**(15): 1475-1485.

Hopfner, K. P. and V. Hornung (2020). "Molecular mechanisms and cellular functions of cGAS-STING signalling." Nat Rev Mol Cell Biol **21**(9): 501-521.

Jackson, S. P. and J. Bartek (2009). "The DNA-damage response in human biology and disease." Nature **461**(7267): 1071-1078.

Jiang, H., X. Xue, S. Panda, A. Kawale, R. M. Hooy, F. Liang, J. Sohn, P. Sung and N. O. Gekara (2019). "Chromatin-bound cGAS is an inhibitor of DNA repair and hence accelerates genome destabilization and cell death." EMBO J **38**(21): e102718.

Jiricny, J. (2006). "The multifaceted mismatch-repair system." Nat Rev Mol Cell Biol **7**(5): 335-346.

Kamphuis, E., T. Junt, Z. Waibler, R. Forster and U. Kalinke (2006). "Type I interferons directly regulate lymphocyte recirculation and cause transient blood lymphopenia." Blood **108**(10): 3253-3261.

Kanayama, M., Y. Izumi, Y. Yamauchi, S. Kuroda, T. Shin, S. Ishikawa, T. Sato, M. Kajita and T. Ohteki (2020). "CD86-based analysis enables observation of bona fide hematopoietic responses." Blood **136**(10): 1144-1154.

Kastenhuber, E. R. and S. W. Lowe (2017). "Putting p53 in Context." Cell **170**(6): 1062-1078.

Kellner, V. and B. Luke (2020). "Molecular and physiological consequences of faulty eukaryotic ribonucleotide excision repair." The EMBO Journal **39**(3): e102309.

Li, T. and Z. J. Chen (2018). "The cGAS-cGAMP-STING pathway connects DNA damage to inflammation, senescence, and cancer." J Exp Med **215**(5): 1287-1299.

Lindahl, T. (2016). "The Intrinsic Fragility of DNA (Nobel Lecture)." Angew Chem Int Ed Engl **55**(30): 8528-8534.

Liu, Y., A. A. Jesus, B. Marrero, D. Yang, S. E. Ramsey, G. A. Montealegre Sanchez, K. Tenbrock, H. Wittkowski, O. Y. Jones, H. S. Kuehn, C.-C. R. Lee, M. A. DiMattia, E. W. Cowen, B. Gonzalez, I. Palmer, J. J. DiGiovanna, A. Biancotto, H. Kim, W. L. Tsai, A. M. Trier, Y. Huang, D. L. Stone, S. Hill, H. J. Kim, C. St. Hilaire, S. Gurprasad, N. Plass, D. Chapelle, I. Horkayne-Szakaly, D. Foell, A. Barysenka, F. Candotti, S. M. Holland, J. D. Hughes, H. Mehmet, A. C. Issekutz, M. Raffeld, J. McElwee, J. R. Fontana, C. P. Minniti, S. Moir, D. L. Kastner, M. Gadina, A. C. Steven, P. T. Wingfield, S. R. Brooks, S. D. Rosenzweig, T. A. Fleisher, Z. Deng, M. Boehm, A. S. Paller and R. Goldbach-Mansky (2014). "Activated STING in a Vascular and Pulmonary Syndrome." New England Journal of Medicine **371**(6): 507-518.

Love, M. I., W. Huber and S. Anders (2014). "Moderated estimation of fold change and dispersion for RNA-seq data with DESeq2." Genome Biology **15**(12): 550.

Luksch, H., W. A. Stinson, D. J. Platt, W. Qian, G. Kalugotla, C. A. Miner, B. G. Bennion, A. Gerbaulet, A. Rosen-Wolff and J. J. Miner (2019). "STING-associated lung disease in mice relies on T cells but not type I interferon." J Allergy Clin Immunol **144**(1): 254-266 e258.

Luksch, H., W. A. Stinson, D. J. Platt, W. Qian, G. Kalugotla, C. A. Miner, B. G. Bennion, A. Gerbaulet, A. Rösen-Wolff and J. J. Miner (2019). "STING-associated lung disease in mice relies on T cells but not type I interferon." Journal of Allergy and Clinical Immunology **144**(1): 254-266.e258.

Mackenzie, K. J., P. Carroll, L. Lettice, Z. Tarnauskaite, K. Reddy, F. Dix, A. Revuelta, E. Abbondati, R. E. Rigby, B. Rabe, F. Kilanowski, G. Grimes, A. Fluteau, P. S. Devenney, R. E. Hill, M. A. Reijns and A. P. Jackson (2016). "Ribonuclease H2 mutations induce a cGAS/STING-dependent innate immune response." EMBO J **35**(8): 831-844.

Mackenzie, K. J., P. Carroll, C. A. Martin, O. Murina, A. Fluteau, D. J. Simpson, N. Olova, H. Sutcliffe, J. K. Rainger, A. Leitch, R. T. Osborn, A. P. Wheeler, M. Nowotny, N. Gilbert, T. Chandra, M. A. M. Reijns and A. P. Jackson (2017). "cGAS surveillance of micronuclei links genome instability to innate immunity." Nature **548**(7668): 461-465.

Mandal, P. K., C. Blanpain and D. J. Rossi (2011). "DNA damage response in adult stem cells: pathways and consequences." Nat Rev Mol Cell Biol **12**(3): 198-202.

McNab, F., K. Mayer-Barber, A. Sher, A. Wack and A. O'Garra (2015). "Type I interferons in infectious disease." Nat Rev Immunol **15**(2): 87-103.

Morcos, M. N. F., C. Li, C. M. Munz, A. Greco, N. Dressel, S. Reinhardt, A. Dahl, N. B. Becker, A. Roers, T. Höfer and A. Gerbaulet (2020). "Hematopoietic lineages diverge within the stem cell compartment." bioRxiv: 2020.2008.2021.261552.

Motwani, M., S. Pawaria, J. Bernier, S. Moses, K. Henry, T. Fang, L. Burkly, A. Marshak-Rothstein and K. A. Fitzgerald (2019). "Hierarchy of clinical manifestations in SAVI N153S and V154M mouse models." Proc Natl Acad Sci U S A **116**(16): 7941-7950.

Ou, H. L. and B. Schumacher (2018). "DNA damage responses and p53 in the aging process." Blood **131**(5): 488-495.

Paludan, S. R., L. S. Reinert and V. Hornung (2019). "DNA-stimulated cell death: implications for host defence, inflammatory diseases and cancer." Nat Rev Immunol **19**(3): 141-153.

Pietras, E. M., R. Lakshminarasimhan, J.-M. Techner, S. Fong, J. Flach, M. Binnewies and E. Passegué (2014). "Re-entry into quiescence protects hematopoietic stem cells from the killing effect of chronic exposure to type I interferons." Journal of Experimental Medicine **211**(2): 245-262.

Reijns, M. A., B. Rabe, R. E. Rigby, P. Mill, K. R. Astell, L. A. Lettice, S. Boyle, A. Leitch, M. Keighren, F. Kilanowski, P. S. Devenney, D. Sexton, G. Grimes, I. J. Holt, R. E. Hill, M. S. Taylor, K. A. Lawson, J. R. Dorin and A. P. Jackson (2012). "Enzymatic removal of ribonucleotides from DNA is essential for mammalian genome integrity and development." Cell **149**(5): 1008-1022.

Roos, W. P., A. D. Thomas and B. Kaina (2016). "DNA damage and the balance between survival and death in cancer biology." Nat Rev Cancer **16**(1): 20-33.

Sangfelt, O., S. Erickson and D. Grander (2000). "Mechanisms of interferon-induced cell cycle arrest." Front Biosci **5**: D479-487.

Sauer, J.-D., K. Sotelo-Troha, J. von Moltke, K. M. Monroe, C. S. Rae, S. W. Brubaker, M. Hyodo, Y. Hayakawa, J. J. Woodward, D. A. Portnoy and R. E. Vance (2011). "The N-Ethyl-N-Nitrosourea-Induced Goldenticket Mouse Mutant Reveals an Essential Function of Sting in the In Vivo Interferon Response to Listeria monocytogenes and Cyclic Dinucleotides." Infection and Immunity **79**(2): 688-694.

Schoggins, J. W., D. A. MacDuff, N. Imanaka, M. D. Gainey, B. Shrestha, J. L. Eitson, K. B. Mar, R. B. Richardson, A. V. Ratushny, V. Litvak, R. Dabelic, B. Manicassamy, J. D. Aitchison, A. Aderem, R. M. Elliott, A. Garcia-Sastre, V. Racaniello, E. J. Snijder, W. M. Yokoyama, M. S. Diamond, H. W. Virgin and C. M. Rice (2014). "Pan-viral specificity of IFN-induced genes reveals new roles for cGAS in innate immunity." Nature **505**: 691.

Schubert, N., T. Schumann, E. Daum, K. Flade, Y. Ge, L. Hagedorn, W. Edelmann, L. Müller, M. Schmitz, G. Kuut, V. Hornung, R. Behrendt and A. Roers (2022). "Genome Replication Is Associated With Release of Immunogenic DNA Waste." Frontiers in Immunology **13**.

Shen, Y. J., N. Le Bert, A. A. Chitre, C. X. Koo, X. H. Nga, S. S. Ho, M. Khatoo, N. Y. Tan, K. J. Ishii and S. Gasser (2015). "Genome-derived cytosolic DNA mediates type I interferon-dependent rejection of B cell lymphoma cells." Cell Rep **11**(3): 460-473.

Stadtfeld, M. and T. Graf (2005). "Assessing the role of hematopoietic plasticity for endothelial and hepatocyte development by non-invasive lineage tracing." Development **132**(1): 203-213.

Subramanian, A., P. Tamayo, V. K. Mootha, S. Mukherjee, B. L. Ebert, M. A. Gillette, A. Paulovich, S. L. Pomeroy, T. R. Golub, E. S. Lander and J. P. Mesirov (2005). "Gene set enrichment analysis: A knowledge-based approach for interpreting genome-wide expression profiles." Proceedings of the National Academy of Sciences **102**(43): 15545-15550.

Takahashi, A., T. M. Loo, R. Okada, F. Kamachi, Y. Watanabe, M. Wakita, S. Watanabe, S. Kawamoto, K. Miyata, G. N. Barber, N. Ohtani and E. Hara (2018). "Downregulation of cytoplasmic DNases is implicated in cytoplasmic DNA accumulation and SASP in senescent cells." Nat Commun **9**(1): 1249.

Vanpouille-Box, C., A. Alard, M. J. Aryankalayil, Y. Sarfraz, J. M. Diamond, R. J. Schneider, G. Inghirami, C. N. Coleman, S. C. Formenti and S. Demaria (2017). "DNA exonuclease Trex1 regulates radiotherapy-induced tumour immunogenicity." Nat Commun **8**: 15618.

Vazquez, S. E., M. A. Inlay and T. Serwold (2015). "CD201 and CD27 identify hematopoietic stem and progenitor cells across multiple murine strains independently of Kit and Sca-1." Exp Hematol **43**(7): 578-585.

Vousden, K. H. and C. Prives (2009). "Blinded by the Light: The Growing Complexity of p53." Cell **137**(3): 413-431.

Warner, J. D., R. A. Irizarry-Caro, B. G. Bennion, T. L. Ai, A. M. Smith, C. A. Miner, T. Sakai, V. K. Gonugunta, J. Wu, D. J. Platt, N. Yan and J. J. Miner (2017). "STING-associated vasculopathy develops independently of IRF3 in mice." J Exp Med **214**(11): 3279-3292.

Williams, J. S., S. A. Lujan and T. A. Kunkel (2016). "Processing ribonucleotides incorporated during eukaryotic DNA replication." Nat Rev Mol Cell Biol **17**(6): 350-363.

Wu, X., V. L. Dao Thi, Y. Huang, E. Billerbeck, D. Saha, H. H. Hoffmann, Y. Wang, L. A. V. Silva, S. Sarbanes, T. Sun, L. Andrus, Y. Yu, C. Quirk, M. Li, M. R. MacDonald, W. M. Schneider, X. An, B. R. Rosenberg and C. M. Rice (2018). "Intrinsic Immunity Shapes Viral Resistance of Stem Cells." Cell **172**(3): 423-438 e425.

Yang, H., H. Wang, J. Ren, Q. Chen and Z. J. Chen (2017). "cGAS is essential for cellular senescence." Proc Natl Acad Sci U S A **114**(23): E4612-E4620.

Yang, M., Q. Liu, T. Niu, J. Kuang, X. Zhang, L. Jiang, S. Li, X. He, L. Wang and J. Li (2020). "Trp53 regulates platelets in bone marrow via the PI3K pathway." Exp Ther Med **20**(2): 1253-1260.

Zierhut, C., N. Yamaguchi, M. Paredes, J. D. Luo, T. Carroll and H. Funabiki (2019). "The Cytoplasmic DNA Sensor cGAS Promotes Mitotic Cell Death." Cell **178**(2): 302-315 e323.

Figure 1 Hematopoietic loss RER results in genome instability and leukemia

A Detection of micronucleated erythrocytes in peripheral blood (PB) of animals with hematopoietic RNase H2 deficiency ($RH2^{hKO}$, right) or Cre-negative controls ($RH2^{hWT}$, left), representative examples of the data in B.

B Frequency of micronucleated erythrocytes among normochromic erythrocytes (n=6-11/genotype, individual mice (15-47 wks of age), means (bars) are shown, significance was calculated by an unpaired Student´s t test).

C Kaplan-Meier survival curve of $RH2^{hKO}$ animals and $RH2^{hWT}$ littermate controls. Significance was calculated by log-rank test.

D Representative example of an enlarged thymus from a leukemic $RH2^{hKO}$ mouse; insets show thymi from either $RH2^{hWT}$ control or non-leukemic $RH2^{hKO}$ animals at the same magnification.

E Thymus weight of leukemic (T-ALL) $RH2^{hKO}$ (n=8), non-leukemic $RH2^{hKO}$ (n=13) and $RH2^{hWT}$ (n=11) mice (aged 6-36 wks).

F-G Representative flow cytometric analysis of total (left) and CD4/8 double-negative (DN, middle) thymocytes as well as PB (G, right) isolated from a leukemic $RH2^{hKO}$ (lower row) and a $RH2^{hWT}$ control (upper row) mouse.

Figure S1 Gating strategies for flow cytometry

A Representative gating strategy for identification of bone marrow hematopoietic stem and progenitor populations (*LS^-K*, lin^- $Sca\text{-}1^-$ $CD117^+$ cells; *LSK*, lin^- $Sca\text{-}1^+$ $CD117^+$ cells; *granulocyte-macrophage progenitor (GMP),* LS^-K $CD16/32^+$ $CD34^+$; *restricted hematopoietic progenitor 1 (HPC-1),* LSK $CD48^{hi}$ $CD150^-$; *restricted hematopoietic progenitor 2 (HPC-2),* LSK $CD48^{hi}$ $CD150^+$; *multipotent progenitor (MPP),* LSK $CD48^{-/lo}$ $CD150^-$; *hematopoietic stem cell (HSC),* LSK $CD48^{-/lo}$ $CD150^+$; *E34 HSC,* LSK $CD48^{-/lo}$ $CD150^+$ $CD34^{-/lo}$ $CD201^{hi}$; *LE^-K*, lin^- $CD201^-$ $CD117^+$ cells; *LEK*, lin^- $CD201^+$ $CD117^+$ cells; *restricted hematopoietic progenitor 1 (HPC-1),* LEK $CD48^{hi}$ $CD150^-$; *restricted hematopoietic progenitor 2 (HPC-2),* LEK $CD48^{hi}$ $CD150^+$; *multipotent progenitor (MPP),* LEK $CD48^{-/lo}$ $CD150^-$; *hematopoietic stem cell (HSC),* LEK $CD48^{-/lo}$ $CD150^+$; *E34 HSC,* LEK $CD48^{-/lo}$ $CD150^+$ $CD34^{-/lo}$ $CD201^{hi}$; percentage of parent populations ± SD was calculated from $RH2^{hWT}$ mice (n=7)). For lineage staining biotin conjugated primary antibodies against murine CD11b, CD8, CD19, NK1.1, Gr-1, CD4, CD3, Ter119 and B220 were used and followed by staining with Streptavidin conjugated with Horizon V500. To block non-specific binding, Rat IgG and an unconjugated anti-mouse CD16/32 antibody were used.

B Representative gating strategy for identification of bone marrow B-lymphocyte populations (*Pre-Pro B-Cells*, $CD19^-$ $B220^+$; *Immature B-Cells*, $CD19^+$ $B220^+$ IgM^+ IgD^-; *Mature B-Cells*, $CD19^+$ $B220^+$ IgM^+ IgD^+; *Pro-B- Cells*, $CD19^+$ $B220^+$ IgM^- IgD^- $CD117^+$ $CD25^-$; *PreBI*, $CD19^+$ $B220^+$ IgM^- IgD^- $CD117^-$ $CD25^-$; *PreBII*, $CD19^+$ $B220^+$ IgM^- IgD^- $CD117^-$ $CD25^+$; percentage of parent populations ± SD was calculated from $RH2^{hWT}$ mice (=7)).

C Representative gating strategy for identification of thymocyte populations (*CD4 single-positive (SP) thymocytes*, $CD4^+$ $CD8^-$; *CD8 SP thymocytes*, $CD4^-$ $CD8^+$; *CD4/8-double positive (DP) thymocytes,* $CD4^+$ $CD8^+$; *CD4/8-double negative (DN) thymocytes,* $CD4^-$ $CD8^-$; *DN1,* $CD4^-$ $CD8^-$ lin^- $CD25^-$ $CD44^+$; *DN2,* $CD4^-$ $CD8^-$ lin^- $CD25^+$ $CD44^+$; *DN3,* $CD4^-$ $CD8^-$ lin^- $CD25^+$ $CD44^-$; *DN4,* $CD4^-$ $CD8^-$ lin^- $CD25^-$ $CD44^-$); percentage of

parent populations ± SD was calculated from $RH2^{hWT}$ mice (n=7)). Lineage staining against B220, NK1.1, CD11b, Gr-1, Ter119, CD19, CD49b surface markers was performed using biotin conjugated antibodies and Streptavidin Horizon V500 as secondary reagent.

D Representative gating strategy for identification of peripheral blood (PB) leukocytes (*neutrophils (Neut)*, $CD11b^{+}$ $Gr1^{hi}$; *B-cells*, $CD11b^{-}$ $GR1^{-}$ $B220^{+}$; *$CD4^{+}$ T-cells,* $CD11b^{-}$ $GR1^{-}$ $B220^{-}$ $CD4^{+}$ $CD8^{-}$ and *$CD8^{+}$ T-cells,* $CD11b^{-}$ $GR1^{-}$ $B220^{-}$ $CD4^{-}$ $CD8^{+}$; percentage of parent populations ± SD was calculated from $RH2^{hWT}$ mice (n=7)).

E Representative gating strategy for identification of micronucleated (MCN) erythrocytes. PB was fixed using -80°C methanol for at least 24h prior to staining. Fixed erythrocytes were digested using RNase A and stained with Ter119, CD71 and PI. Nucleated leukocytes (≥2N DNA content) and $CD71^{+}$ reticulocytes were discriminated and normochromic (NC, $CD71^{-}$) erythrocytes were analysed for micronuclei (PI^{+}, percentage of parent populations ± SD was calculated from $RH2^{hWT}$ mice (n=7)).

Figure S2 Hematopoietic loss RER results in genome instability and leukemia

A Body weight of age- and sex-matched, non-leukemic $RH2^{hKO}$ (closed circles) and $RH2^{hWT}$ (open circles) mice (aged 6-16 wks, n=12-17/group). Significance was calculated using an unpaired student's t-test.

B-C Representative micrographs of spleens (upper row) and thymi (lower row) isolated from $RH2^{hWT}$ (left), leukemic $RH2^{hKO}$ (middle) and undiseased $RH2^{hKO}$ (right) animals. Sections were stained by May-Grünwald-Giemsa.

Figure 2 Chronic genome damage impairs blood cell production and HSC fitness

A PB cell counts of $RH2^{hKO}$ (closed circles) and Cre-negative controls ($RH2^{hWT}$, open circles). Erythrocyte (RBC), B cell, CD4/CD8 T lymphocyte, neutrophil (Neut), and platelet (PLT) numbers were determined (n=13-18/genotype, individual mice and means (bars) are shown, cell numbers were normalized to $RH2^{hWT}$ ctrl means (set to 1, dotted line), unpaired Student´s t test with Holm-Sidak post test).

B Absolute numbers of bone marrow hematopoietic stem and progenitor cells (BM HSPCs) were determined (HSCs, LEK $CD48^{-/lo}CD150^{+}$), multipotent (MPP, LEK $CD48^{-}CD150^{-}$) hematopoietic progenitor cells HPC-1 (LEK $CD48^{+}CD150^{-}$), erythro-myeloid progenitors ($LE^{-}K$) progenitors and whole bone marrow cellularity (WBMC) were determined (n=4-7/genotype; display, normalization and significance of data as in A).

C Numbers of developing B lymphocyte progenitors in the bone marrow. (n=4-7/genotype; display, normalization and significance of data as in A).

D Thymocyte development (DN: CD4/CD8 double-negative; DP: double-positive; SP: single-positive; n=4-7/genotype; display, normalization and significance of data as in A).

E-F Single HSCs ($LSKCD48^{-/lo}CD150^{+}CD34^{-/lo}CD201^{hi}$, n=38-44) isolated from either $RH2^{hKO}$ or $RH2^{hWT}$ mice were cultivated in presence of IL-3, TPO, SCF and EPO. (E) Cells were counted for 96h every 12h, mean & SD are shown, significance was calculated by repeated measures 2-way ANOVA with Sidak post test). (F) Colony size after 10 days of culture (median and individual colonies are shown, significance was calculated by Mann-Whitney U test).

G-I 200 $RH2^{hKO}$ (closed symbols, solid line) or $RH2^{hWT}$ (open symbols, dotted line) HSCs (LEK $CD48^{-/lo}CD150^{+}$) were mixed with 500,000 WT B6.CD45.1 WBMCs and competitively transplanted into lethally irradiated B6.CD45.1/CD45.2 recipient mice (G, n=6-7/genotype). Donor chimerism of PB neutrophils (Neut, square), B (circle) and T (triangle) cells (H, mean and SD is shown, significance was calculated by repeated measures 2-way ANOVA with Sidak post test) and BM LSK cells (I, individual mice & means (bars) are shown, significance was calculated by an unpaired Student´s t test) was quantified.

Figure S3 Chronic genome damage impairs blood cell production and HSC fitness

A Representative example of thymi isolated from an un-diseased $RH2^{hKO}$ (left) or $RH2^{hWT}$ (right) mouse (scale bar 5 mm).

B, C Weight of thymi (B, n=9-10/genotype) and spleens (C, n=14-16/genotype) isolated from un-diseased $RH2^{hKO}$ mice and $RH2^{hWT}$ littermates (age 8-16 wks, individuals & means (bars) are shown, significance was calculated by an un-paired Student´s t test).

D-I Few $RH2^{hKO}$ mice exhibited ameliorated cytopenia and were designated as "$RH2^{hKO}$ rescue" (grey circles). PB (D), HSPC (E), B lymphocyte (F) and thymocyte (G) counts; same $RH2^{hKO}$ and $RH2^{hWT}$ animals, display and normalization of data as in Figure 2A-D. (H) Percentages of micronucleated erythrocytes (I) Median fluorescence intensity (MFI) of Sca-1 surface expression among HSCs (LEK $CD48^{-/lo}$ $CD150^{+}$).

J-K $5x10^{6}$ WBMCs were isolated from primary recipients of either $RH2^{hKO}$ or $RH2^{hWT}$ HSCs (shown in Figure 2H-I) and serially transplanted into lethally irradiated secondary recipients (n=6/genotype). PB (J) and BM LSK (K) chimerism are shown (display of data and statistic as in Figure 2H-I).

Figure 3 Genome damage in $RH2^{hKO}$ mice activates p53 and type I IFN signaling

A-D Transcriptome analysis of BM granulocyte-macrophage progenitors (GMP, $LE^{-}K$ $CD16/32^{+}CD34^{+}$) isolated from $RH2^{hKO}$ (n=4) and $RH2^{hWT}$ control (n=4) mice revealed 218 differential expressed genes (false discovery rate (FDR) 5%). (A) Volcano plot (B) Differentially expressed interferon (IFN) stimulated genes (ISGs) and (C) p53 DNA repair pathway genes. (D) Gene set enrichment analysis showed upregulation of genes involved in p53, apoptosis, NFκB and IFNα signaling in $RH2^{hKO}$ mice.

E Sca-1 expression of PB T lymphocytes determined by FACS (n=3-6/genotype, individual mice & means are shown, unpaired Student´s t test)

Figure S4 Genome damage in $RH2^{hKO}$ mice activates p53 and type I IFN signaling

A-B Expression of ISGs was determined by quantitative reverse transcription (qRT)-PCR in BM cells (A) and splenocytes (B) isolated from $RH2^{hKO}$ (individual mice and means (bars) are shown) and $RH2^{hWT}$ control mice (dotted line).

C Surface Sca-1 expression was determined on HSCs (LEK $CD48^{-/lo}$ $CD150^{+}$, significance was calculated by unpaired Student´s t test).

Figure 4 Attenuation of the p53 response rescues the hematopoietic defects of $RH2^{hKO}$ mice

A-B PB and BM of $RH2^{hKO}$ mice with additional heterozygous loss of p53 ($RH2^{hKO}$*Trp53*$^{KO/WT}$, red closed triangles) were analyzed. Cell counts were normalized to $RH2^{hWT}$*Trp53*$^{WT/WT}$ controls (open circles). Individual mice and means (bars) are shown, significance was calculated by 1way ANOVA with Holm-

Sidak post test, RH2^{hKO}*Trp53*$^{WT/WT}$ (black asterisks) and RH2^{hKO}*Trp53*$^{KO/WT}$ (red asterisks) were compared to RH2^{hWT}*Trp53*$^{WT/WT}$ control mice, while significant differences between both RH2^{hKO} groups are underscored. PB cell counts (A) and absolute numbers of BM HSPC populations (B) isolated from 2 femora, 2 tibiae, and 2 pelvis are shown.

C-F Competitive transplantation of HSCs (LEK CD48$^{-/lo}$CD150^{+}) isolated from either RH2^{hKO}*Trp53*$^{KO/WT}$, RH2^{hKO}*Trp53*$^{WT/WT}$ or RH2^{hWT}*Trp53*$^{WT/WT}$ mice. Each lethally-irradiated B6.CD45.1/CD45.2 recipient was i.v. injected with 200 donor HSCs mixed with 500,000 B6.CD45.1 BM competitor cells. PB neutrophil (Neut, C), B- (D) and T-cell (E) donor chimerism of primary recipients was determined (n=6-7 recipients/genotype, means & SD are shown, was calculated by repetitive measures 2way ANOVA with Holm-Sidak post test). 22 weeks after transplantation, the donor chimerism of BM LSK cells was analyzed (F, see Figure S5C-F for 2ndary transplantation).

G The percentage of micronucleated erythrocytes was determined (individuals and means (bars) are shown, significance was calculated by 1way ANOVA with Holm Sidak post test).

H Sca-1 median fluorescence intensity of CD8^{+} T cells from peripheral blood was analyzed (individuals and means (bars) are shown, significance was calculated by 1way ANOVA with Holm Sidak post test).

Figure S5

A-B Thymocyte (A) and BM B cell (B) development (display and normalization of data and statistics as in Figure 4A-B).

C-F 5 x 10^{6} whole bone marrow cells isolated from each primary recipients (Figure 4C-F) were transplanted into a sex-matched secondary recipients. Chimerism of neutrophils (C), B- (D) and T- (E) cells isolated from peripheral blood (Mean and SD are shown, significance was calculated by repeated measures 2way ANOVA with Holm Sidak post test, comparison between RH2^{hKO} p53$^{WT/WT}$ and RH2^{hKO} p53$^{KO/WT}$ is shown in brown lettering). (F) BM LSK chimerism 14 weeks after secondary transplantation (individual mice and means (bars) are shown, 1way ANOVA with Holm-Sidak post test).

G Sca-1 MFI of HSCs (LEK CD48$^{-/lo}$CD150^{+}) was calculated (individuals and means (bar) shown. Significance was calculated by 1way ANOVA with Holm-Sidak post test

Figure 5 Loss of one functional Trp53 allele accelerates leukemogenesis of RH2^{hKO} mice

A Kaplan Meier survival plot, significance was calculated by log-rank test (### = RH2^{hKO}*Trp53*$^{WT/WT}$ vs. RH2^{hKO}*Trp53*$^{KO/WT}$, ***= RH2^{hKO}*Trp53*$^{WT/WT}$ vs. RH2^{hWT}*Trp53*$^{WT/WT}$).

B Splenomegaly in a diseased RH2^{hKO}p53$^{KO/WT}$ mouse (bar = 5 mm, spleens from RH2^{hWT} and non-leukemic RH2^{hKO}p53$^{KO/WT}$ mice are shown for comparison).

C Spleen histology (May-Grünwald Giemsa) from a representative RH2^{hKO}*Trp53*$^{KO/WT}$ mouse diagnosed with AML-like disease and control animals.

D Expansion of BM lin^{-}CD117^{hi}Sca-1^{-} cells (left dot plot), that disseminated to PB (middle dot plot) and spleen (right dot plot). Lower row depicts RH2^{hWT} control animal.

E Distribution of disease entities in RH2^{hKO}*Trp53*$^{WT/WT}$ (n=8) and RH2^{hKO}*Trp53*$^{KO/WT}$ (n=13) diagnosed with leukemia.

Figure S6 Loss of Trp53 accelerates leukemogenesis of RH2^{hKO} mice

A Immuno-phenotypical characterization of leukemic BM cells isolated from a representative RH2^{hKO}*Trp53*$^{KO/WT}$ mouse diagnosed with AML and un-diseased controls (Upper row shows lineage-negative BM cells, lower row show histograms of lineage^{-}CD201^{-}Kit^{hi} (LE-K) cells. Fluorescence minus-one controls served as negative controls).

B-I Phenotypical characterization of hematopoietic RNASEH2 KO mice with homozygous p53 deficiency. All RH2^{hKO}*Trp53*$^{KO/KO}$ animals (n=4) already showed development of leukemia by 8 weeks of age. (B) Representative dot plots of thymocyte suspensions isolated from and RH2^{hKO}p53$^{KO/KO}$ animals. (C-G) RH2^{hWT}*Trp53*$^{WT/WT}$ (n=3), RH2^{hKO}*Trp53*$^{WT/WT}$ (n=4) and RH2^{hKO}*Trp53*$^{KO/KO}$ (n=3) mice (8 wks of age) were analyzed by flow cytometry. PB (C), BM HSPC (D), BM B lymphocyte (E) and thymocyte (F) development are shown. Individual mice and means (bars) are shown, data was normalized to RH2^{hWT} control (set to 1), significance was calculated using 1way Anova with Holm-Sidak post test. (G) Sca-1 expression of CD8+ T-cells (significance was calculated by 1way ANOVA).

Figure 6 Signaling via the cGAS/STING axis has no impact on RER-deficient hematopoiesis

A Upregulation of the ISG Sca-1 was determined on PB CD8^{+} T cells isolated from RH2^{hKO} mice with an additional loss of either cGAS (*Cgas*$^{KO/KO}$), IFNAR (*Ifnar1*$^{KO/KO}$) or STING (*Sting1*$^{GT/GT}$). RH2^{hKO} and RH2^{hWT} animals served as controls; data was normalized to the mean MFI of RH2^{hWT} mice, individual mice and means (bars) are shown, significance of either RH2^{hWT} or RH2^{hKO} animals versus double KO mice was calculated by 1way ANOVA with Holm-Sidak post test.

B-E Numbers of PB erythrocytes (B), B- (C), T-lymphocytes (D) and platelets (E). Normalization and display of data as in A.

F-I Competitive transplantation of 200 purified HSCs (LEK CD48$^{-/lo}$CD150^{+}) isolated from either Cre-negative (ctrl), RH2^{hKO} single KO or indicated double KO mice and injected together with 500,000 WT B6 CD45.1 BM competitor cells. The donor chimerism of PB neutrophils (Neut, F), B- (G) and T-cells (H) was determined (n=6-7 recipients/genotype, means & SD are shown, significance between RH2^{hKO} and double KO mice was calculated by RM 2way ANOVA with Holm-Sidak post test. (I) Chimerism of BM LEK cells 23 weeks after transplantation. Significance was calculated by 1way ANOVA with Holm-Sidak post test.

J-K Single HSCs (LSK CD48$^{-/lo}$CD150^{+}CD34$^{-/lo}$CD201^{hi}, n=44-72/genotype & time point) were isolated from either RH2^{hWT}*Sting1*$^{GT/GT}$ (n=2), RH2^{hKO}*Sting1*$^{WT/WT}$ (n=3) or RH2^{hKO}*Sting1*$^{GT/GT}$ (n=3) mice and cultivated for 10 days, (J) mean cell count & SD are shown, repeated measures 2-way ANOVA with Holm-Sidak post test. (K) Colony size after 10 days of culture (median and individual colonies are shown, significance was calculated by 1way ANOVA with Holm-Sidak post test).

L Percentage of micronucleated erythrocytes was determined (individual mice and means (bars) are shown, significance was calculated by 1way ANOVA with Holm-Sidak post test).

M Kaplan-Meier survival curves of RH2^{hKO} mice with an additional loss of either cGAS, IFNAR or STING as well as RH2^{hKO} and RH2^{hWT} control animals (significance was calculated by log-rank test.)

N Leukemia entities observed in RH2^{hKO} mouse strains with or without additional KO (number of diagnosed cases is given for each strain).

Figure S7 Signaling via the cGAS/STING axis has no impact on RER-deficient hematopoiesis
A Numbers of PB neutrophils. Normalization and display of data as in Figure 6A-E.

B-C BM B lymphocyte (B) and thymocyte (C) development of $RH2^{hKO}$ mice with additional loss of STING ($RH2^{hKO}$*Sting1*$^{GT/GT}$) were analyzed. Cell counts were normalized to $RH2^{hWT}$*Sting1*$^{WT/WT}$ controls (set to 1, dotted line). Individual mice and means (bars) are shown, significance was calculated by 1way ANOVA with Holm-Sidak post test.

D The frequencies of micronucleated PB erythrocytes were determined (individual mice are shown, statistical analysis was performed using 1Way ANOVA followed by Holm-Sidak Post test).

Figure 7 Loss of cGAS does not alter steady state or stress hematopoiesis
A, B Single HSCs (LSK $CD48^{-/lo}CD150^{+}CD34^{-/lo}CD201^{hi}$, n=70-103/condition-) isolated from *Cgas*$^{KO/KO}$ (red) or WT control (black) mice were cultivated for 10 days. A fraction of cells was exposed to 2 Gy γ-radiation (triangles) before culture. (A) Cells were counted for 96h every 24h (means & SD are shown, 2-way ANOVA with Sidak post test). (B) Colony size after 10 days of culture (medians and individual colonies are shown, significance was calculated by Mann-Whitney U test, pooled data from 2 individual experiments, mean colony size of un-irradiated *Cgas*$^{WT/WT}$ mice was set to 1).

C-F 50 HSCs (LSK $CD48^{-/lo}CD150^{+}$ $CD201^{hi}$) were isolated either from *Cgas*$^{KO/KO}$ (red, n=5) or WT control (black, n=5) donor mice, mixed with 200,000 B6.CD45.1 WBMCs and competitively transplanted into lethally irradiated recipients (n=6-8/condition). Two additional recipient cohorts were transplanted with donor HSCs that received 2 Gy of γ-irradiation *ex vivo* (triangles). PB neutrophil (C), B- (D)and T- (E) lymphocyte chimerism of primary recipients was determined (means & SD are shown, significance was calculated by repeated measures 2way ANOVA). (F) Chimerism of BM LSK cells 18 weeks after transplantation (individual mice and means (bars) shown, significance was determined by 1way ANOVA with Sidak-Holm post test).

G-J *Cgas*$^{KO/KO}$ mice (red, n=6) and *Cgas*$^{WT/WT}$ littermate controls (black, n=6) were exposed to 2 Gy γ-radiation. PB was repeatedly sampled, median Sca-1 fluorescence intensity of $CD8^{+}$ T cells (G), leukocyte (H, WBC), reticulocyte (I, RET) and platelet (J, PLT) numbers were measured (means and SD shown, significance was calculated by repeated measures 2way ANOVA with Holm-Sidak post test).

K-N *Cgas*$^{KO/KO}$ mice (red, n=6) and *Cgas*$^{WT/WT}$ littermate controls (black, n=6) were injected with 5-FU. Display of data and statistics as in G-J.

O-P *Cgas*$^{KO/KO}$ mice (red, n=6) and *Cgas*$^{WT/WT}$ littermate controls (black, n=6) were exposed to 9 Gy γ-radiation, sacrificed 10h later and BM was analyzed. Mature (O) and lineage-negative (P) BM populations were analyzed. Absolute cell counts from 2 femora were determined and normalized to un-irradiated control (set to 1, dotted line), individual mice and means (bars) are shown, significance was calculated by an unpaired Student´s t test.

Figure S8 Loss of cGAS does not alter steady state or stress hematopoiesis
A-B BM HSPCs from *Cgas*$^{KO/KO}$ (red) and *Cgas*$^{WT/WT}$ (black) animals were analyzed (n=3/genotype, individual and means (bars) shown, aged 11-14 wks, significance was calculated by an unpaired Student´s t test). (A) Percentages of HSPCs among lineage negative BM cells (mean of WT control was set to 1). (B) Sca-1 expression was determined on BM LEK cells.

C-D Peripheral blood cell counts (C) and Sca-1 expression among CD8 T cells (D) were determined (normalized to WT (1), n=16-18/genotype, data from 3 independent experiments, significance was calculated by an unpaired Student´s t test, aged 9-16 wks).

E, F (E) BM was analyzed in aged *Cgas*$^{KO/KO}$ (red) and *Cgas*$^{WT/WT}$ (black) animals (n=3/genotype, age 48-52 wks, significance was calculated by an unpaired Student´s t test).(E) Percentage of HSPCs among lineage negative BM (mean of WT control was set to 1). (F) Sca-1 expression was determined on BM LEK cells.

G, H Single HSCs (LSK CD48$^{-/lo}$CD150^{+}CD34$^{-/lo}$CD201^{hi}) isolated from aged (48-52 wks, n=3/genotype) *Cgas*$^{KO/KO}$ (red) or WT control (black) mice were cultivated for 10 days. A fraction of cells was exposed to 2 Gy γ-radiation (triangles) before culture. (G) Cells were counted for 96h every 12h (means & SD are shown, 2-way ANOVA with Sidak post test). (H) Colony size after 10 days of culture (medians and individual colonies are shown, significance was calculated by Mann-Whitney U test).

I-L *Cgas*$^{KO/KO}$ mice (red, n=6) and *Cgas*$^{WT/WT}$ littermate controls (black, n=6) were exposed to 2 Gy γ-radiation (same mice as Figure 7G-J). BM HSPC numbers (I), Sca-1 expression on LEK E34 HSCs (J), BM B lymphocyte numbers (K) and thymocyte frequencies (L) were determined 15 days after irradiation (individual animals and means (bars) are shown, mean of WT was set to 1 (except for J), significance was calculated by an unpaired Students t test).

M-P *Cgas*$^{KO/KO}$ mice (red, n=6) and *Cgas*$^{WT/WT}$ littermate controls (black, n=6) were injected with 5-FU (same animals as in Figure 7K-N). Display of data and statistics as in Figure S7I-L.

Q *Cgas*$^{KO/KO}$ mice (red, n=6) and *Cgas*$^{WT/WT}$ littermate controls (black, n=6) were exposed to 9 Gy γ-radiation, sacrificed 10h later and BM was analyzed (same mice as in Figure 7O-P). Representative example of gating for lineage^{-}CD201^{+}CD117^{+} (LEK) cells (upper row, PI^{-}lineage^{-} BM cells pre-gated) and LEK CD48$^{-/lo}$CD150^{+} cells (lower row). Percentage among viable BM cells is given.

Figure 8 Chronic STING activation by SAVI-associated gain-of-function mutation massively impairs HSC potential

A, B Single HSCs (LSK CD48$^{-/lo}$CD150^{+}CD34$^{-/lo}$ CD201^{hi}, n=83-91) isolated from either *Sting1*$^{N153S/WT}$*Ifnar1*$^{KO/KO}$ mice (N153S, n=3) or *Sting1*$^{WT/WT}$*Ifnar1*$^{KO/KO}$ littermate controls (WT, n=3) were cultivated for 10 days. (A) Cells were counted by light microscopy every 12h (mean& SD are shown, significance was calculated by 2way ANOVA with Sidak-Holm post test). (B) Colony size after 10 days of culture (individual colonies & medians (bars) are shown, significance was calculated by Mann-Whitney U test).

C, D Competitive transplantation of *Sting1*$^{N153S/WT}$*Ifnar1*$^{KO/KO}$ (N153S, solid lines, closed symbols) or *Sting1*$^{WT/WT}$*Ifnar1*$^{KO/KO}$ (WT, dashed lines, open symbols) HSCs into lethally irradiated WT recipients (n=3-4/genotype & timepoint). (C) Donor chimerism of PB neutrophils (Neut, red circles), B- (blue triangles) and T-lymphocytes (green squares) was determined. Left plot shows primary transplantation (1° TX). 5x10^{6} WBMCs from primary recipients were serially transplanted into secondary recipients (2° TX, right plot). (D) BM HSC chimerism of secondary recipients.

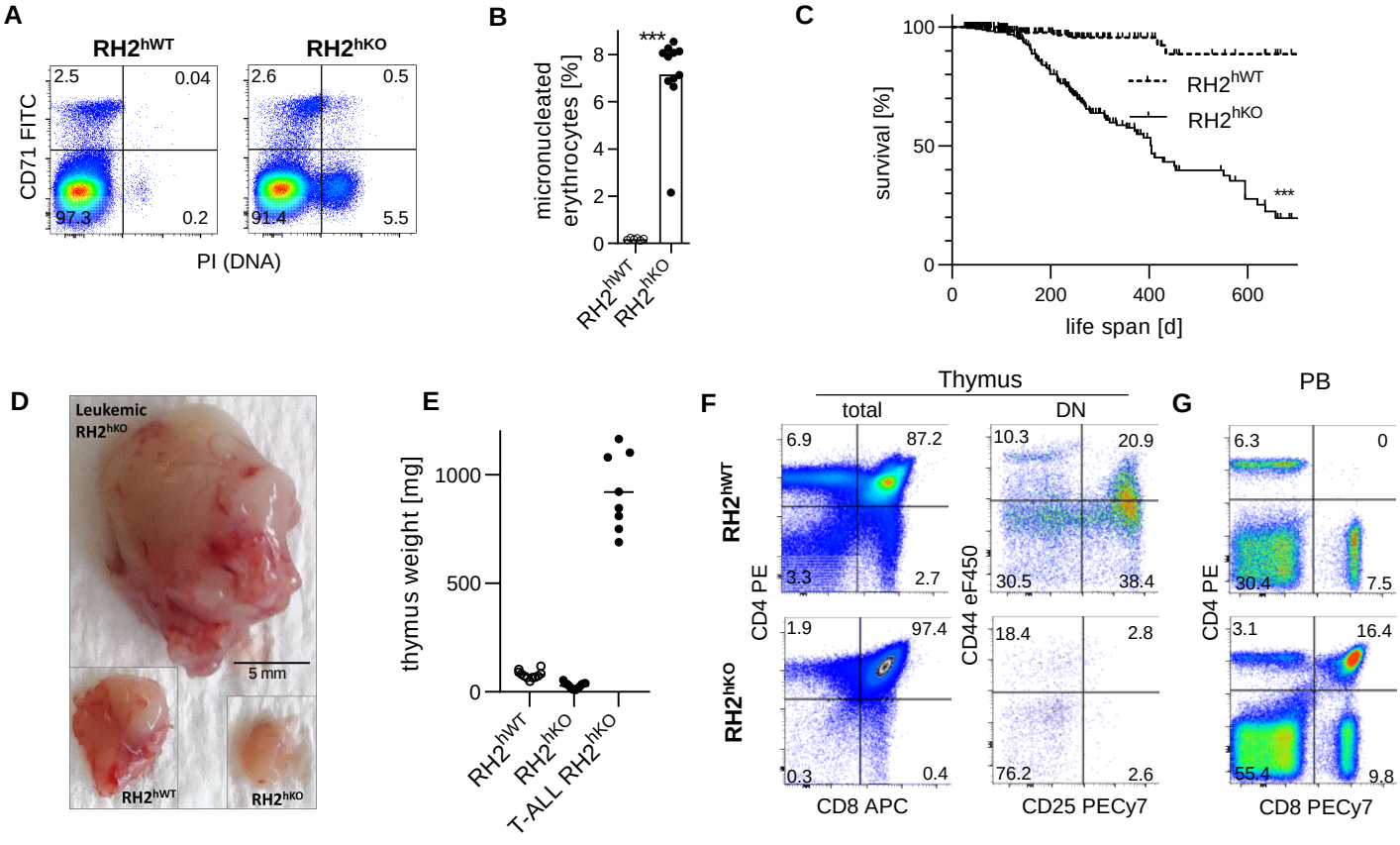
A
RH2hWT
RH2hKO
2.5
0.04
97.3
0.2
2.6
0.5
91.4
5.5
CD71 FITC
PI (DNA)
B
micronucleated erythrocytes [%]
***
RH2hWT
RH2hKO
C
survival [%]
RH2hWT
RH2hKO
***
life span [d]
D
Leukemic RH2hKO
5 mm
RH2hWT
RH2hKO
E
thymus weight [mg]
RH2hWT
RH2hKO
T-ALL RH2hKO
F
Thymus
total
DN
RH2hWT
RH2hKO
6.9
87.2
3.3
2.7
10.3
20.9
30.5
38.4
1.9
97.4
0.3
0.4
18.4
2.8
76.2
2.6
CD4 PE
CD44 eF450
CD8 APC
CD25 PECy7
G
PB
6.3
0
30.4
7.5
3.1
16.4
55.4
9.8
CD4 PE
CD8 PECy7

Figure 1

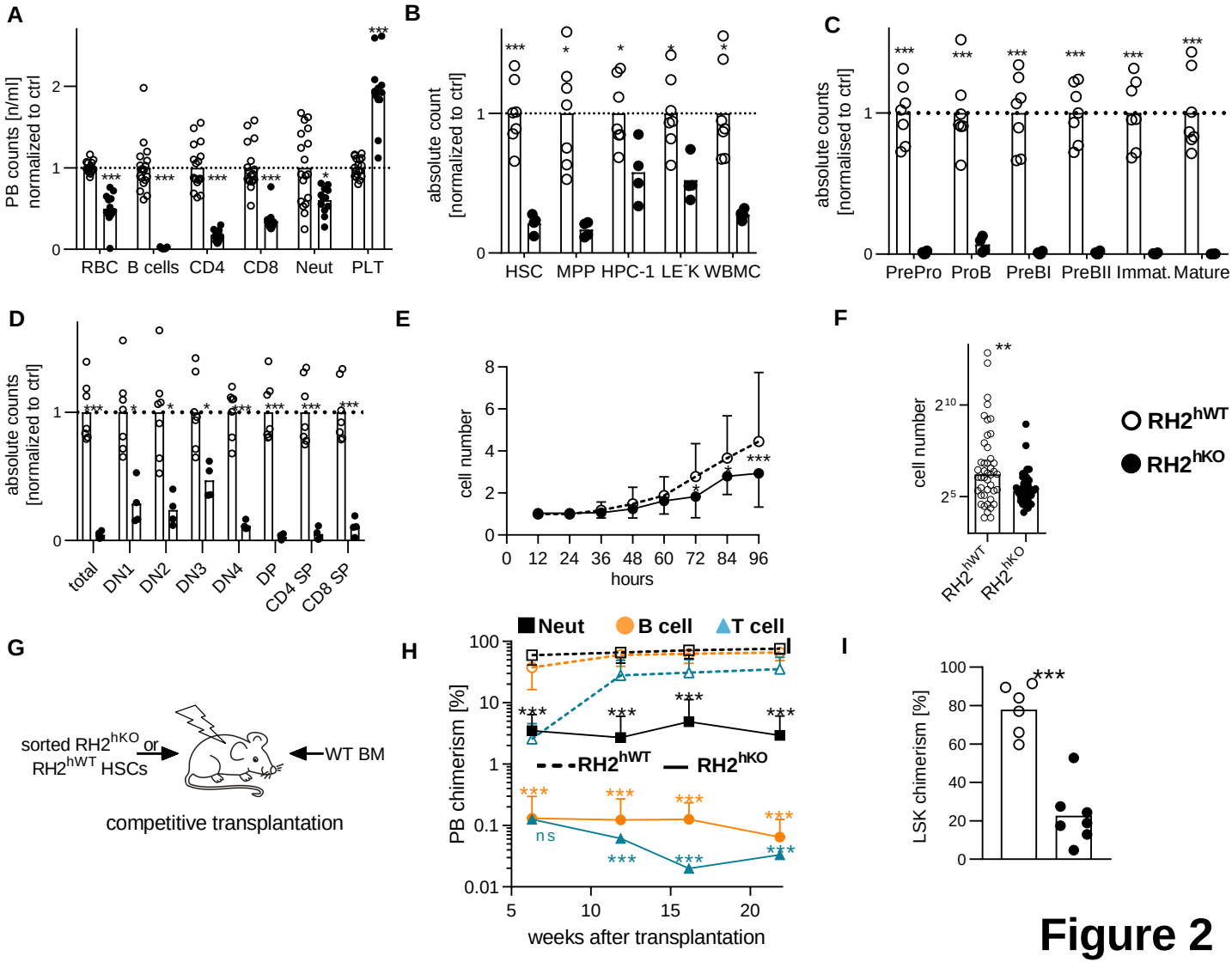
A
PB counts [n/ml] normalized to ctrl
RBC
B cells
CD4
CD8
Neut
PLT
B
absolute count [normalized to ctrl]
HSC
MPP
HPC-1
LE⁻K
WBMC
C
absolute counts [normalised to ctrl]
PrePro
ProB
PreBI
PreBII
Immat.
Mature
D
absolute counts [normalized to ctrl]
total
DN1
DN2
DN3
DN4
DP
CD4 SP
CD8 SP
E
cell number
hours
F
cell number
RH2hWT
RH2hKO
G
sorted RH2hKO or RH2hWT HSCs
WT BM
competitive transplantation
H
Neut
B cell
T cell
PB chimerism [%]
RH2hWT
RH2hKO
ns
weeks after transplantation
I
LSK chimerism [%]

Figure 2

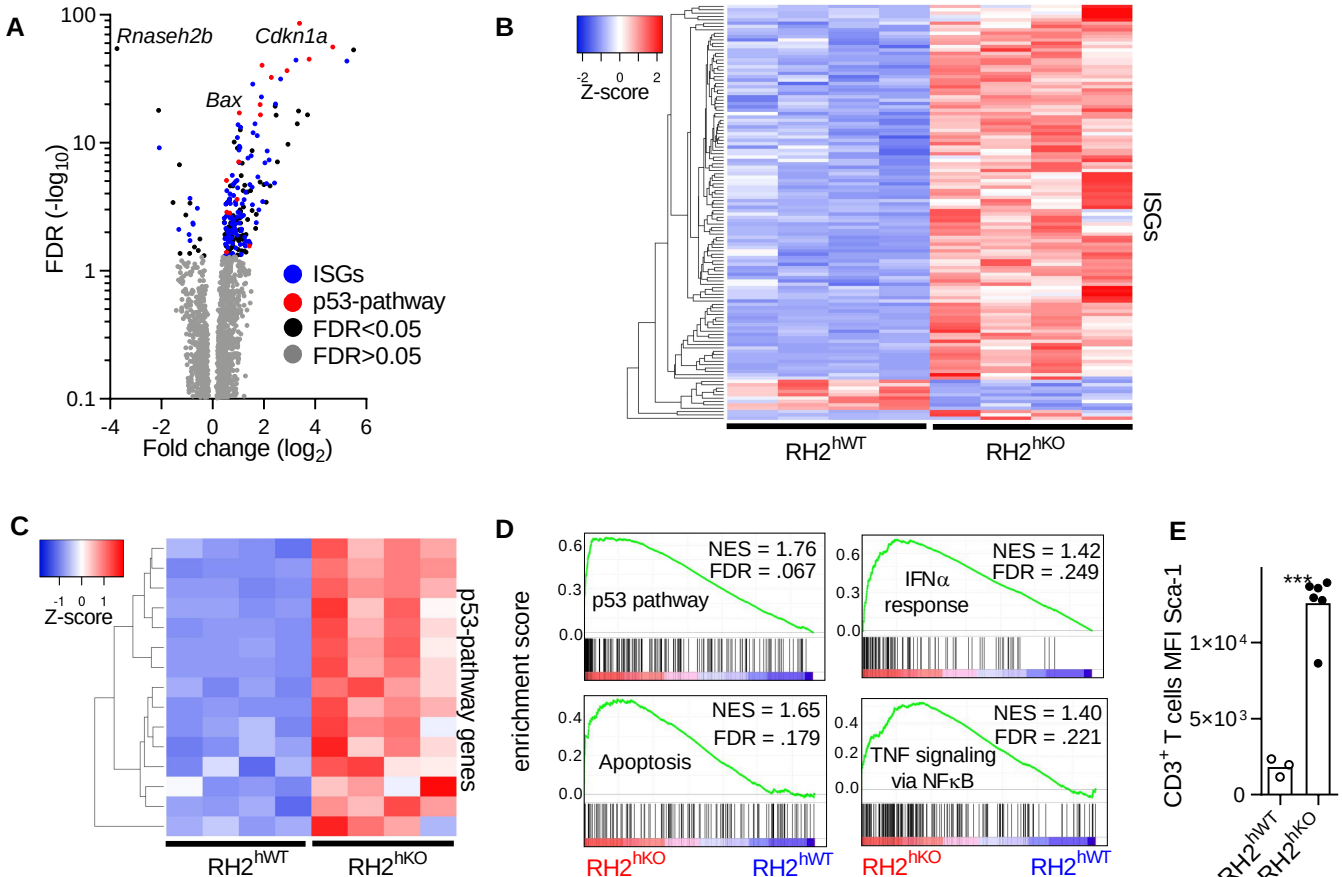
A
Rnaseh2b
Cdkn1a
Bax
FDR (-log10)
100
10
1
0.1
-4
-2
0
2
4
6
Fold change (log2)
ISGs
p53-pathway
FDR<0.05
FDR>0.05
B
Z-score
-2
0
2
ISGs
RH2hWT
RH2hKO
C
Z-score
-1
0
1
p53-pathway genes
RH2hWT
RH2hKO
D
enrichment score
NES = 1.76
FDR = .067
p53 pathway
NES = 1.42
FDR = .249
IFNα
response
NES = 1.65
FDR = .179
Apoptosis
NES = 1.40
FDR = .221
TNF signaling
via NFκB
RH2hKO
RH2hWT
E
CD3+ T cells MFI Sca-1
***
1×10^4
5×10^3
0
RH2hWT
RH2hKO

Figure 3

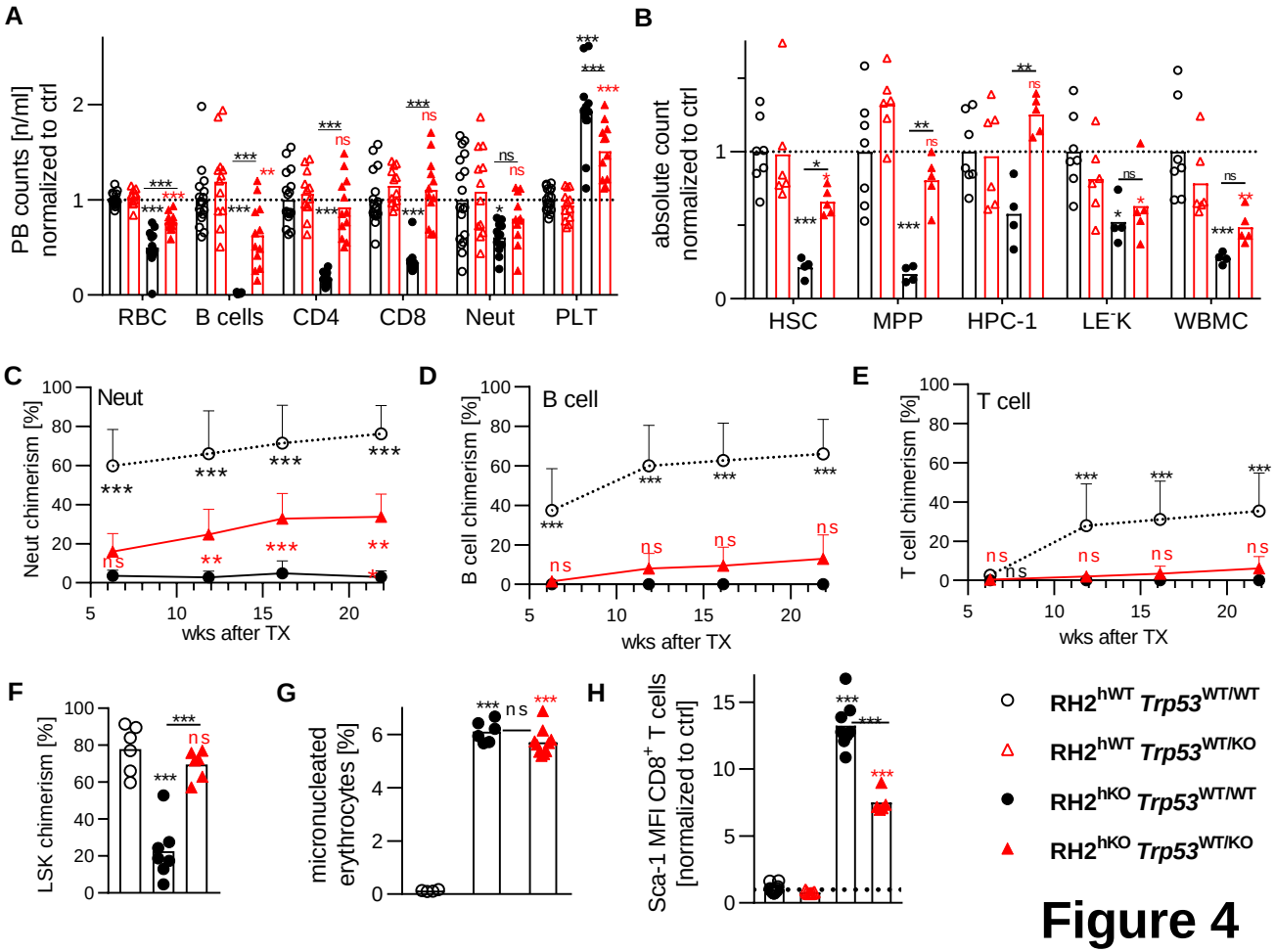
A
PB counts [n/ml] normalized to ctrl
RBC
B cells
CD4
CD8
Neut
PLT
B
absolute count normalized to ctrl
HSC
MPP
HPC-1
LE⁻K
WBMC
C
Neut
Neut chimerism [%]
wks after TX
D
B cell
B cell chimerism [%]
wks after TX
E
T cell
T cell chimerism [%]
wks after TX
F
LSK chimerism [%]
G
micronucleated erythrocytes [%]
H
Sca-1 MFI CD8+ T cells [normalized to ctrl]
RH2hWT Trp53WT/WT
RH2hWT Trp53WT/KO
RH2hKO Trp53WT/WT
RH2hKO Trp53WT/KO

Figure 4

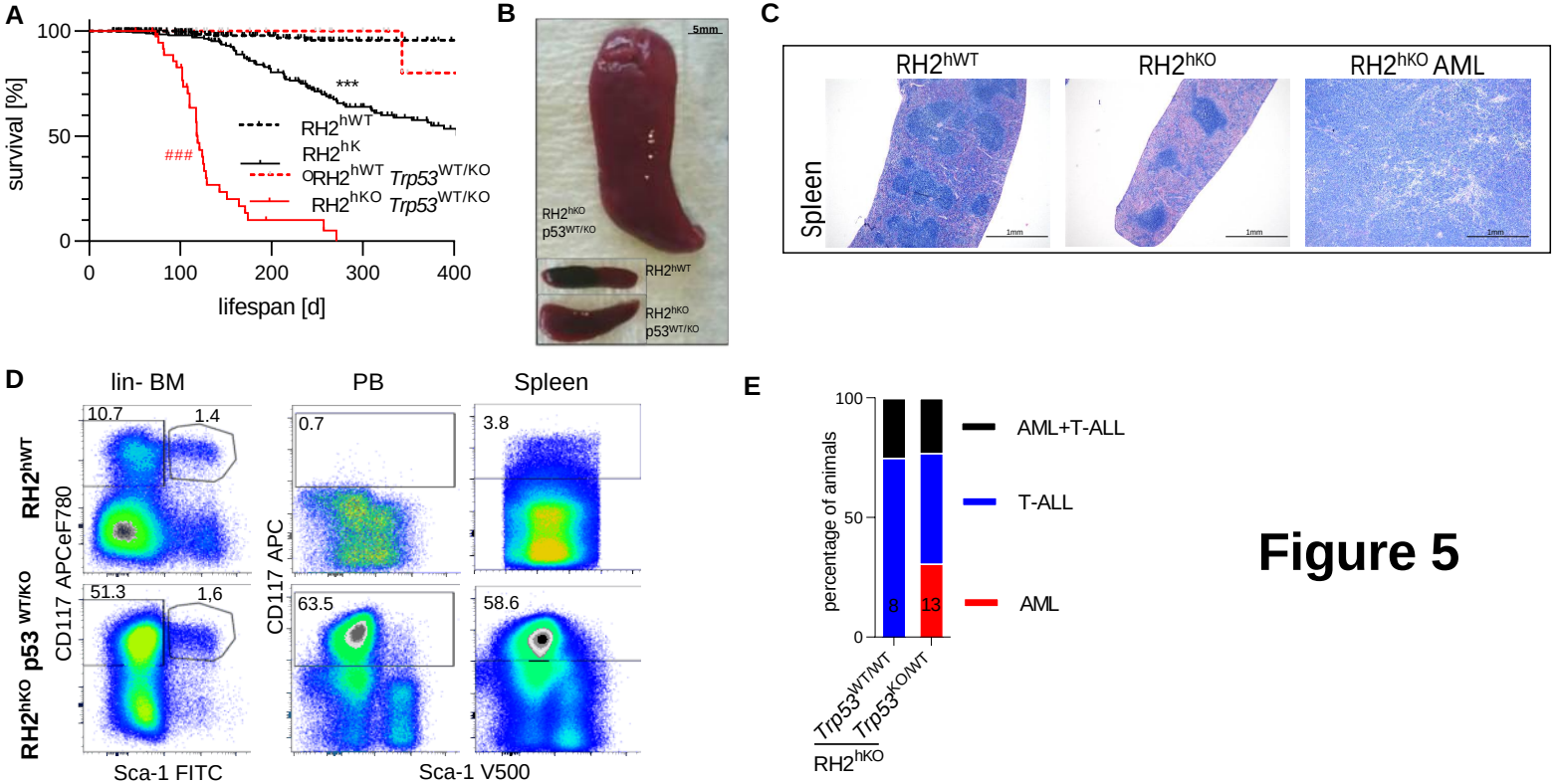
A
100
50
0
survival [%]
0
100
200
300
400
lifespan [d]
***
###
RH2hWT
RH2hK
RH2hWT Trp53WT/KO
RH2hKO Trp53WT/KO
B
5mm
RH2hKO
p53WT/KO
RH2hWT
RH2hKO
p53WT/KO
C
RH2hWT
RH2hKO
RH2hKO AML
Spleen
1mm
D
lin- BM
PB
Spleen
RH2hWT
RH2hKO p53WT/KO
CD117 APCeF780
CD117 APC
10.7
1.4
0.7
3.8
51.3
1.6
63.5
58.6
Sca-1 FITC
Sca-1 V500
E
100
50
0
percentage of animals
6
13
AML+T-ALL
T-ALL
AML
Trp53WT/WT
Trp53KO/WT
RH2hKO

Figure 5

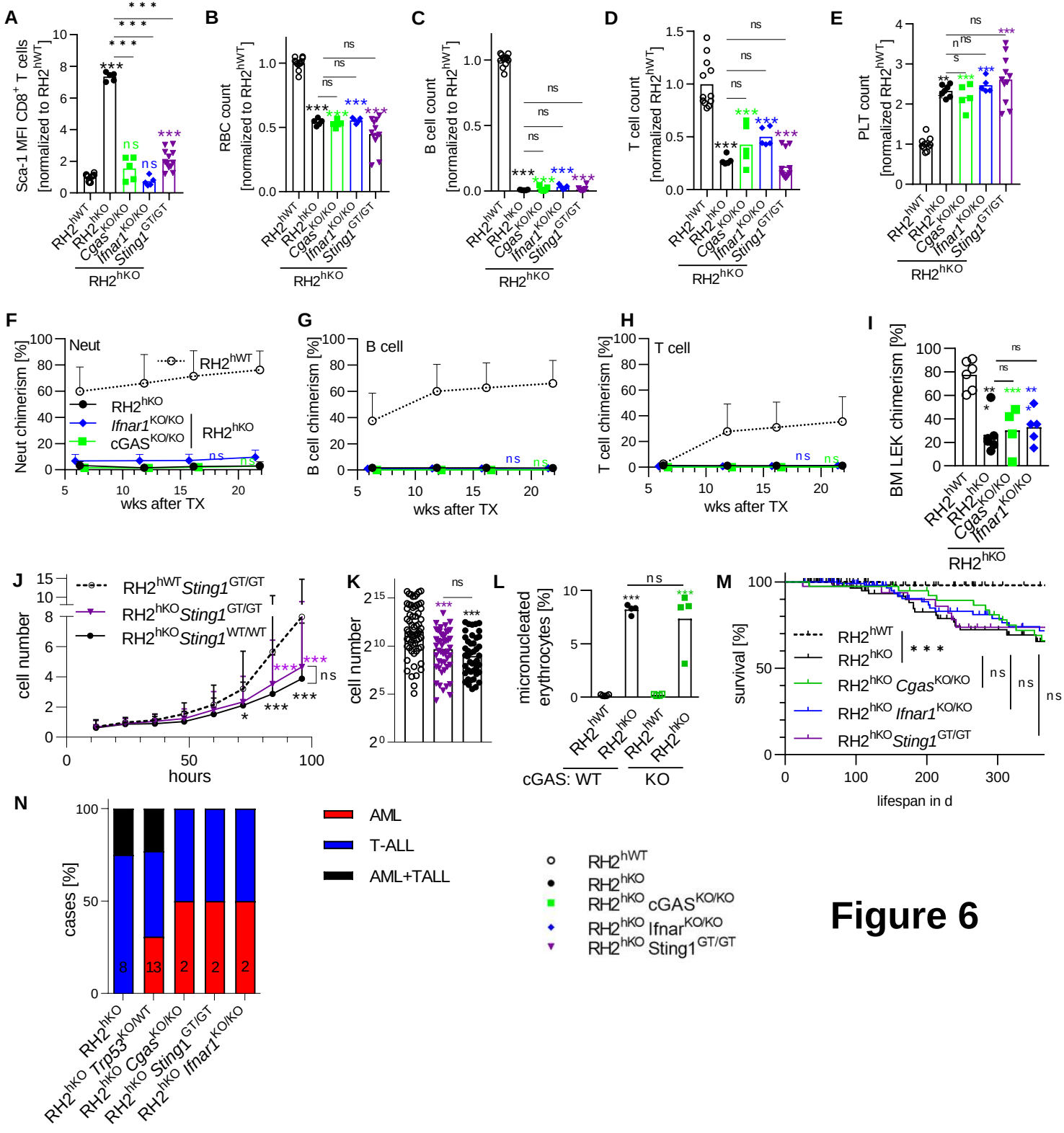
A
Sca-1 MFI CD8+ T cells [normalized to RH2hWT]
B
RBC count [normalized to RH2hWT]
C
B cell count [normalized to RH2hWT]
D
T cell count [normalized RH2hWT]
E
PLT count [normalized RH2hWT]
RH2hWT
RH2hKO
Cgas KO/KO
Ifnar1 KO/KO
Sting1 GT/GT
RH2hKO
F
Neut chimerism [%]
Neut
RH2hWT
RH2hKO
Ifnar1 KO/KO
cGAS KO/KO
RH2hKO
wks after TX
G
B cell chimerism [%]
B cell
wks after TX
H
T cell chimerism [%]
T cell
wks after TX
I
BM LEK chimerism [%]
RH2hKO
J
cell number
RH2hWT Sting1 GT/GT
RH2hKO Sting1 GT/GT
RH2hKO Sting1 WT/WT
hours
K
cell number
L
micronucleated erythrocytes [%]
cGAS: WT
KO
M
survival [%]
RH2hWT
RH2hKO
RH2hKO Cgas KO/KO
RH2hKO Ifnar1 KO/KO
RH2hKO Sting1 GT/GT
lifespan in d
N
cases [%]
AML
T-ALL
AML+TALL
8
13
2
2
2
RH2hKO
RH2hKO Trp53 KO/WT
RH2hKO Cgas KO/KO
RH2hKO Sting1 GT/GT
RH2hKO Ifnar1 KO/KO
RH2hWT
RH2hKO
RH2hKO cGAS KO/KO
RH2hKO Ifnar KO/KO
RH2hKO Sting1 GT/GT

Figure 6

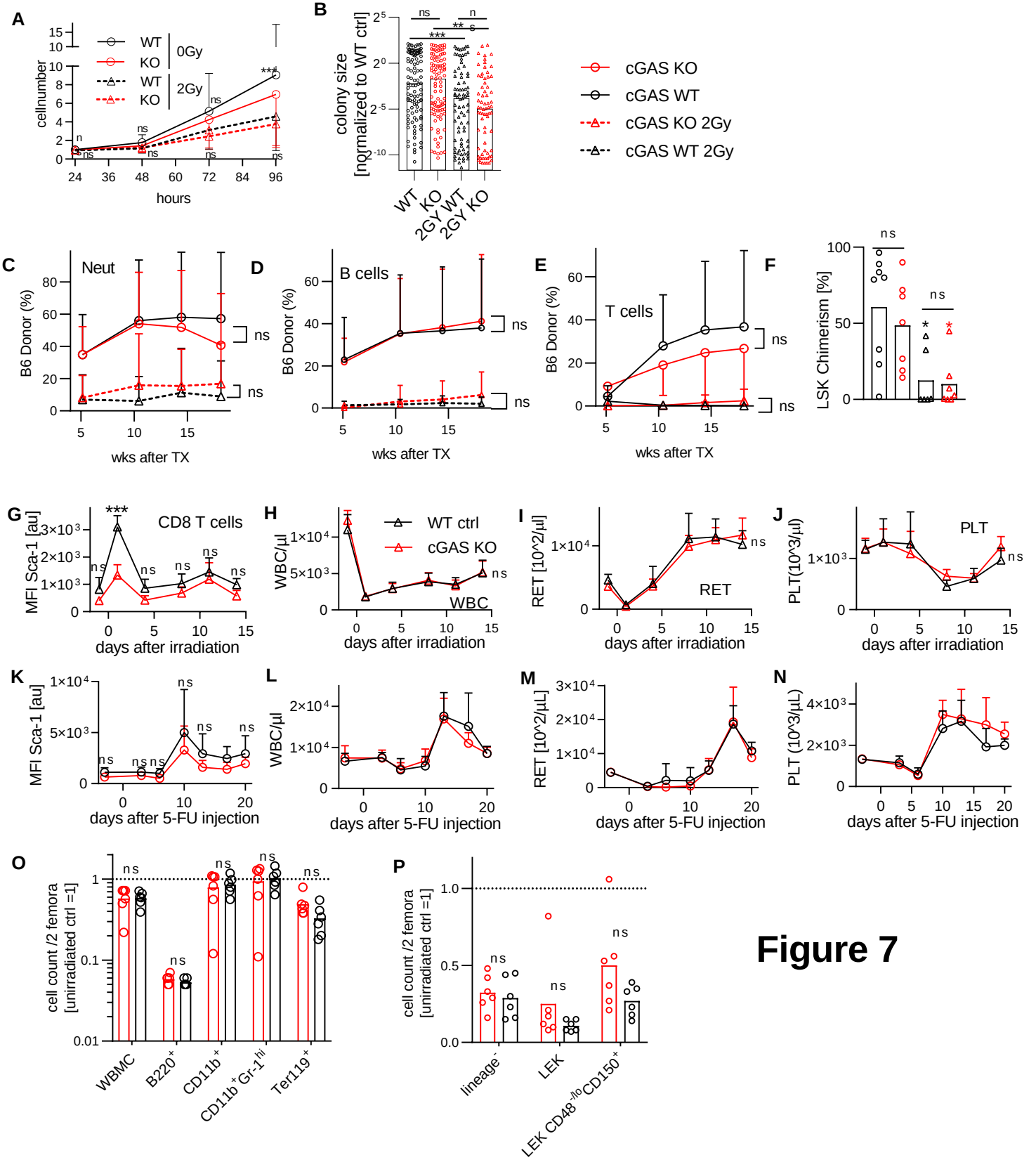
A
cellnumber
hours
WT
KO
0Gy
2Gy
B
colony size [normalized to WT ctrl]
WT
KO
2GY WT
2GY KO
cGAS KO
cGAS WT
cGAS KO 2Gy
cGAS WT 2Gy
C
Neut
B6 Donor (%)
wks after TX
D
B cells
E
T cells
F
LSK Chimerism [%]
G
CD8 T cells
MFI Sca-1 [au]
days after irradiation
H
WBC/µl
WT ctrl
cGAS KO
WBC
I
RET [10^2/µl]
RET
J
PLT(10^3/µl)
PLT
K
days after 5-FU injection
L
M
N
O
cell count /2 femora [unirradiated ctrl =1]
WBMC
B220+
CD11b+
CD11b+Gr-1hi
Ter119+
P
lineage-
LEK
LEK CD48-/loCD150+

Figure 7

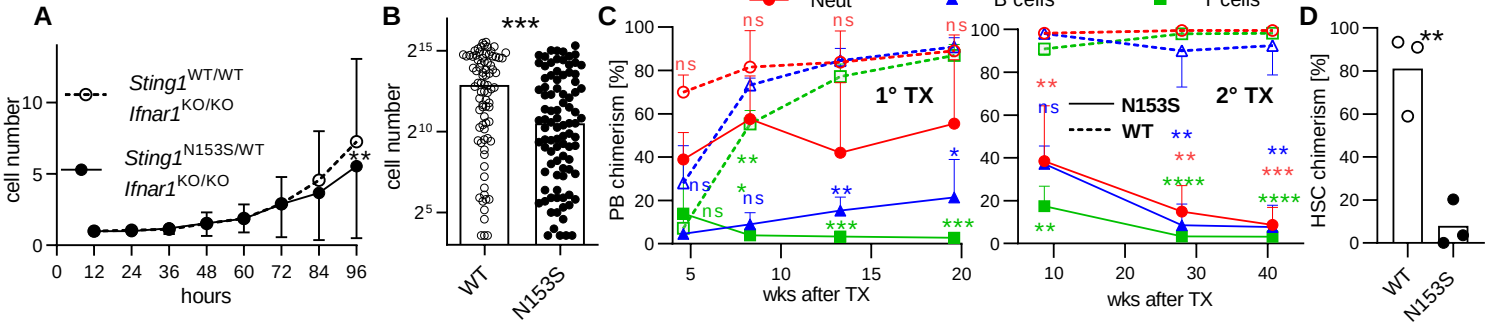
A
cell number
Sting1WT/WT
Ifnar1KO/KO
Sting1N153S/WT
Ifnar1KO/KO
**
hours
B
***
cell number
WT
N153S
C
Neut
B cells
T cells
PB chimerism [%]
1° TX
2° TX
N153S
WT
wks after TX
wks after TX
D
**
HSC chimerism [%]
WT
N153S

Figure 8

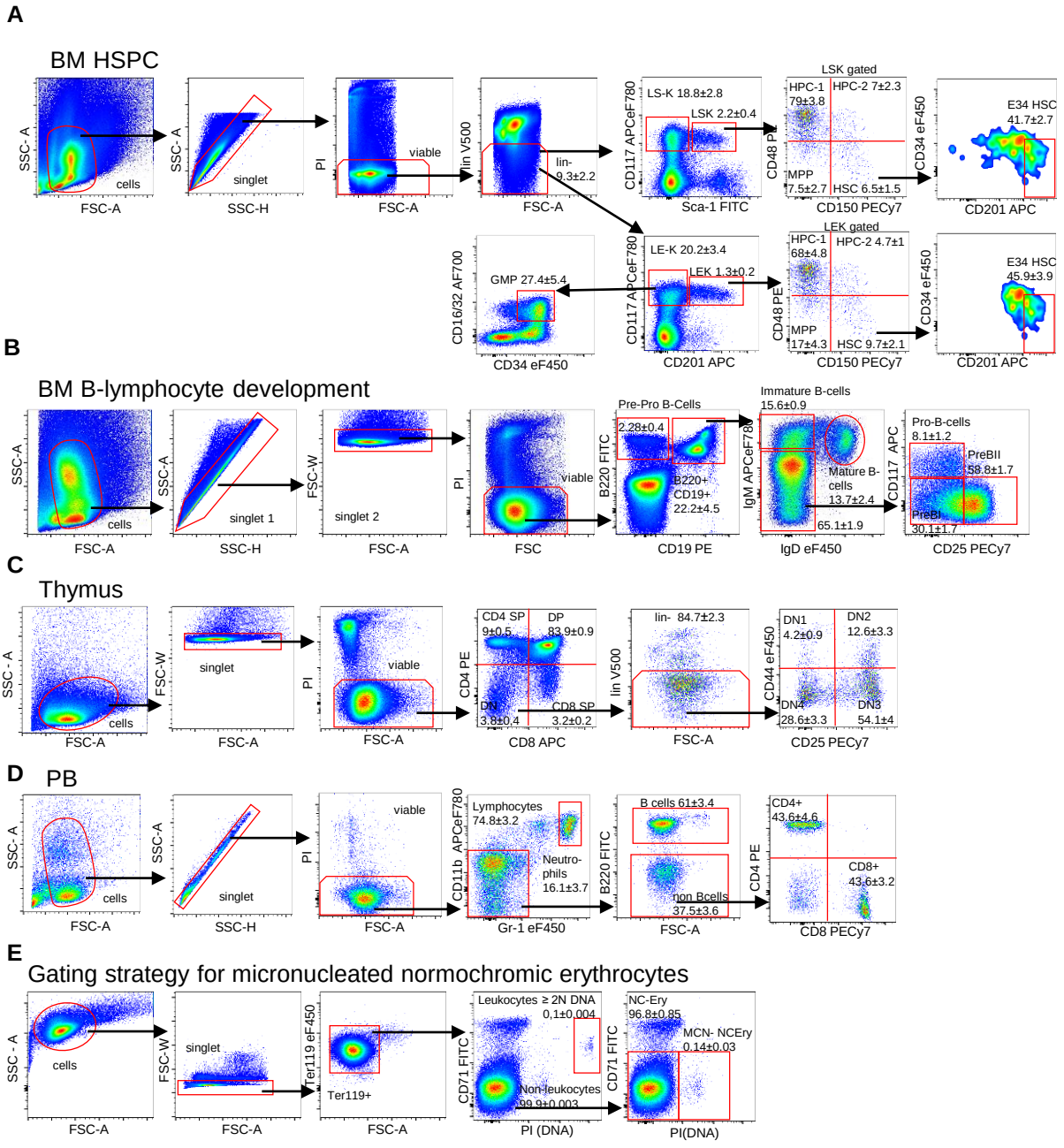

Figure S1

A

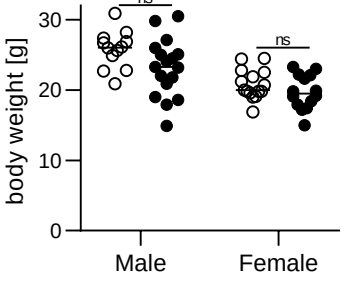
ns
ns
30
20
10
0
body weight [g]
Male
Female

B

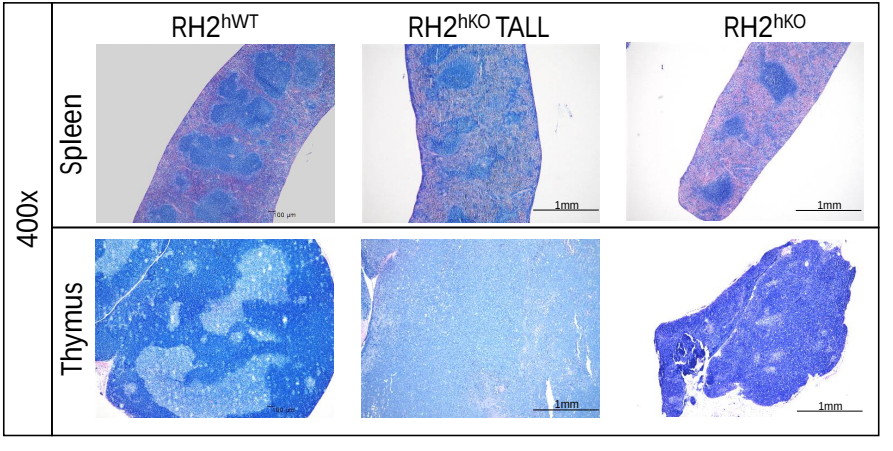
RH2hWT
RH2hKO TALL
RH2hKO
400x
Spleen
Thymus
1mm
1mm
1mm
1mm

Figure S2

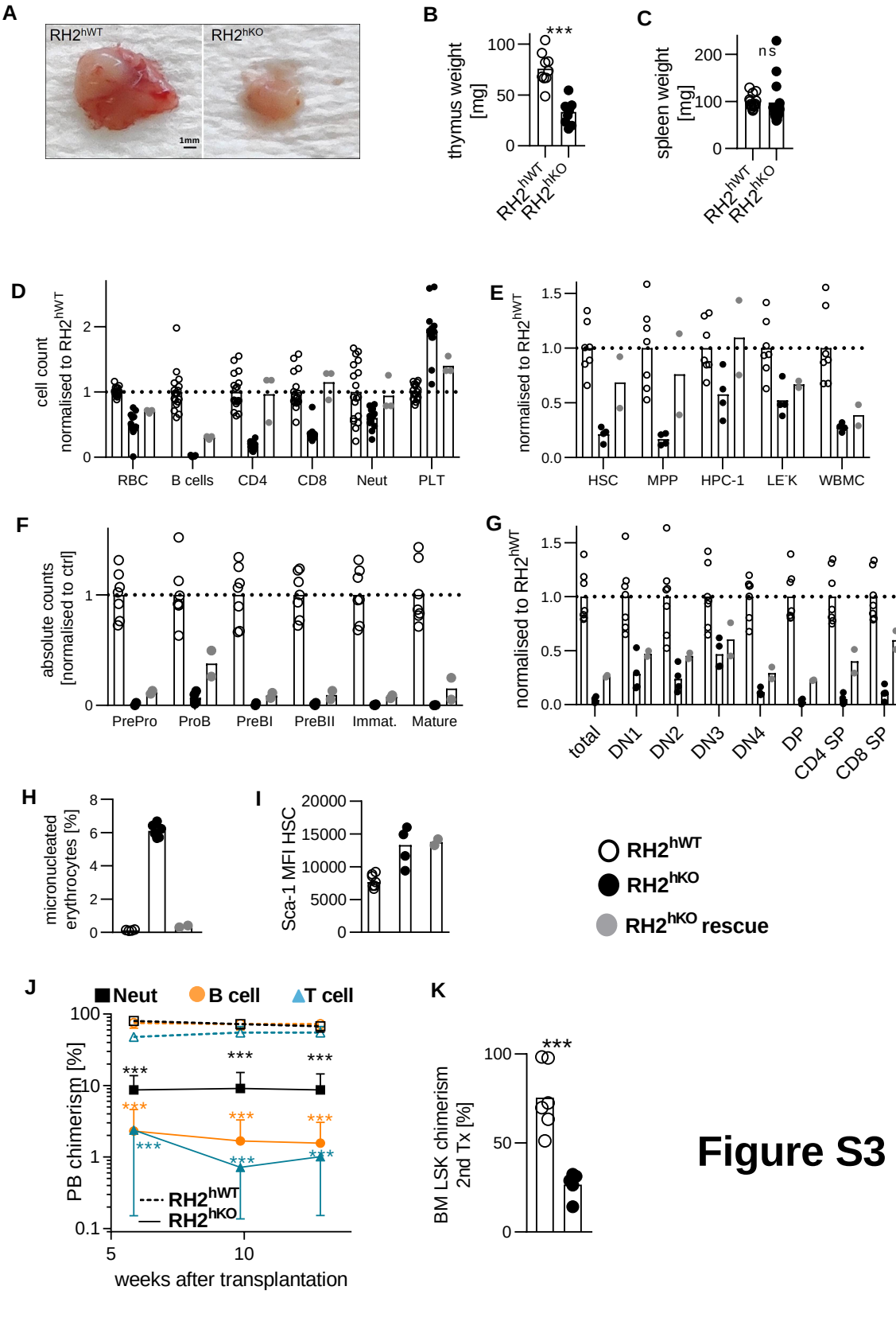
A
RH2hWT
RH2hKO
1mm
B
thymus weight [mg]
***
RH2hWT
RH2hKO
C
spleen weight [mg]
ns
D
cell count normalised to RH2hWT
RBC
B cells
CD4
CD8
Neut
PLT
E
normalised to RH2hWT
HSC
MPP
HPC-1
LE-K
WBMC
F
absolute counts [normalised to ctrl]
PrePro
ProB
PreBI
PreBII
Immat.
Mature
G
normalised to RH2hWT
total
DN1
DN2
DN3
DN4
DP
CD4 SP
CD8 SP
H
micronucleated erythrocytes [%]
I
Sca-1 MFI HSC
RH2hWT
RH2hKO
RH2hKO rescue
J
Neut
B cell
T cell
PB chimerism [%]
RH2hWT
RH2hKO
weeks after transplantation
K
BM LSK chimerism 2nd Tx [%]

Figure S3

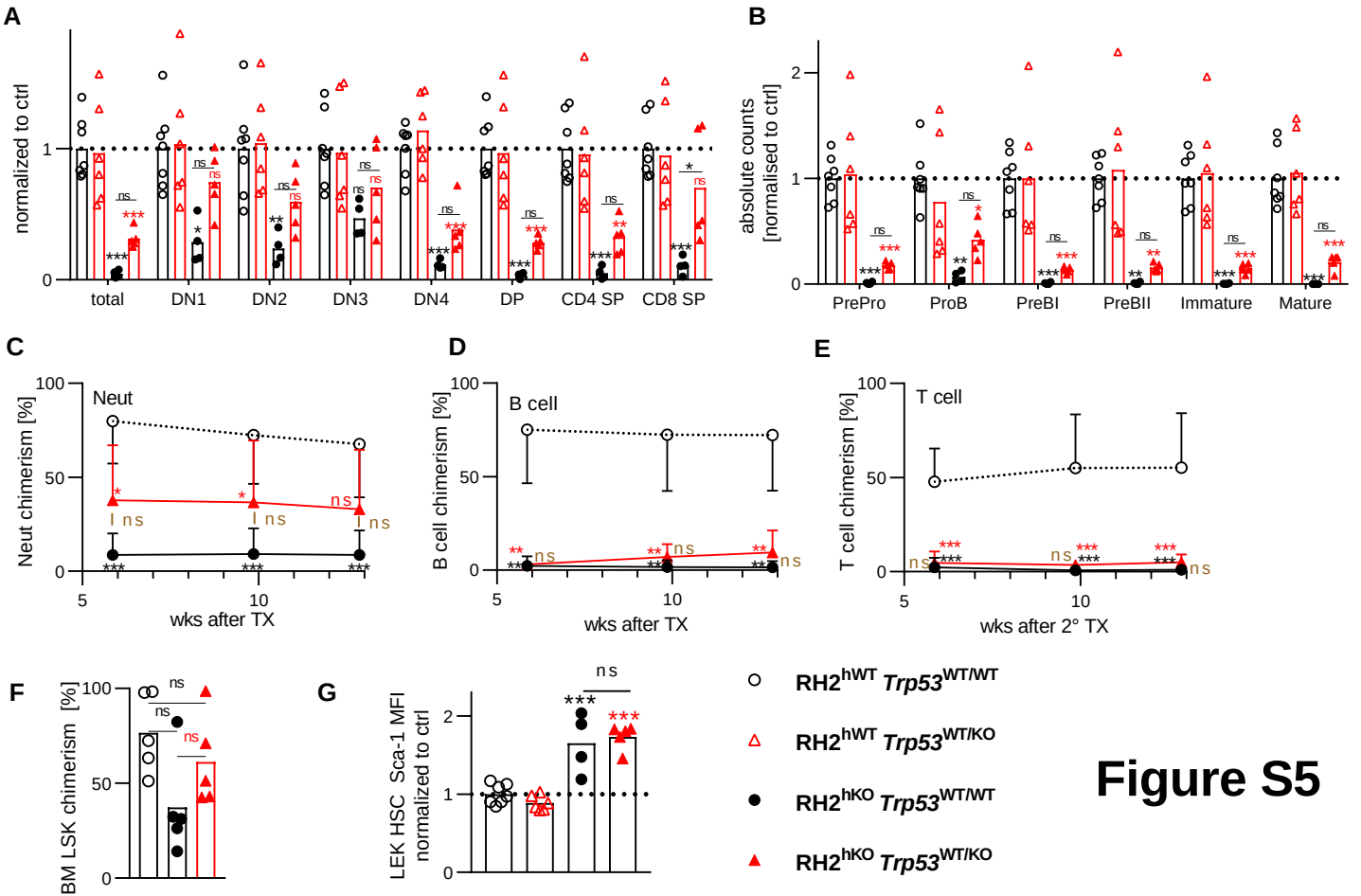
A
normalized to ctrl
total
DN1
DN2
DN3
DN4
DP
CD4 SP
CD8 SP
B
absolute counts [normalised to ctrl]
PrePro
ProB
PreBI
PreBII
Immature
Mature
C
Neut
Neut chimerism [%]
wks after TX
D
B cell
B cell chimerism [%]
wks after TX
E
T cell
T cell chimerism [%]
wks after 2° TX
F
BM LSK chimerism [%]
G
LEK HSC Sca-1 MFI normalized to ctrl
RH2hWT Trp53WT/WT
RH2hWT Trp53WT/KO
RH2hKO Trp53WT/WT
RH2hKO Trp53WT/KO

Figure S5

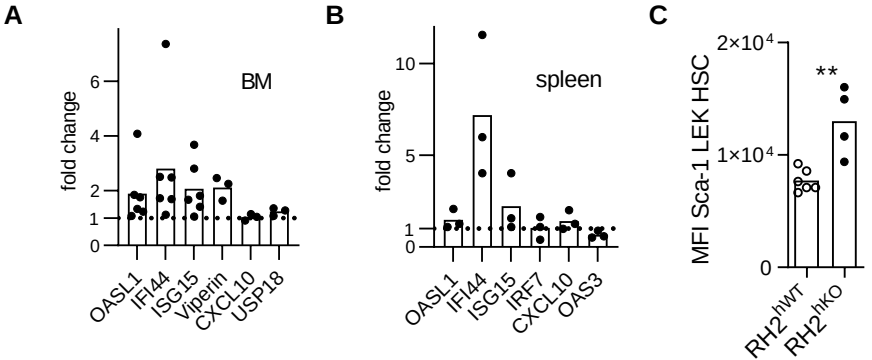
A
fold change
BM
0
1
2
4
6
OASL1
IFI44
ISG15
Viperin
CXCL10
USP18
B
fold change
spleen
0
1
5
10
OASL1
IFI44
ISG15
IRF7
CXCL10
OAS3
C
MFI Sca-1 LEK HSC
2×10⁴
1×10⁴
0
**
RH2hWT
RH2hKO

Figure S4

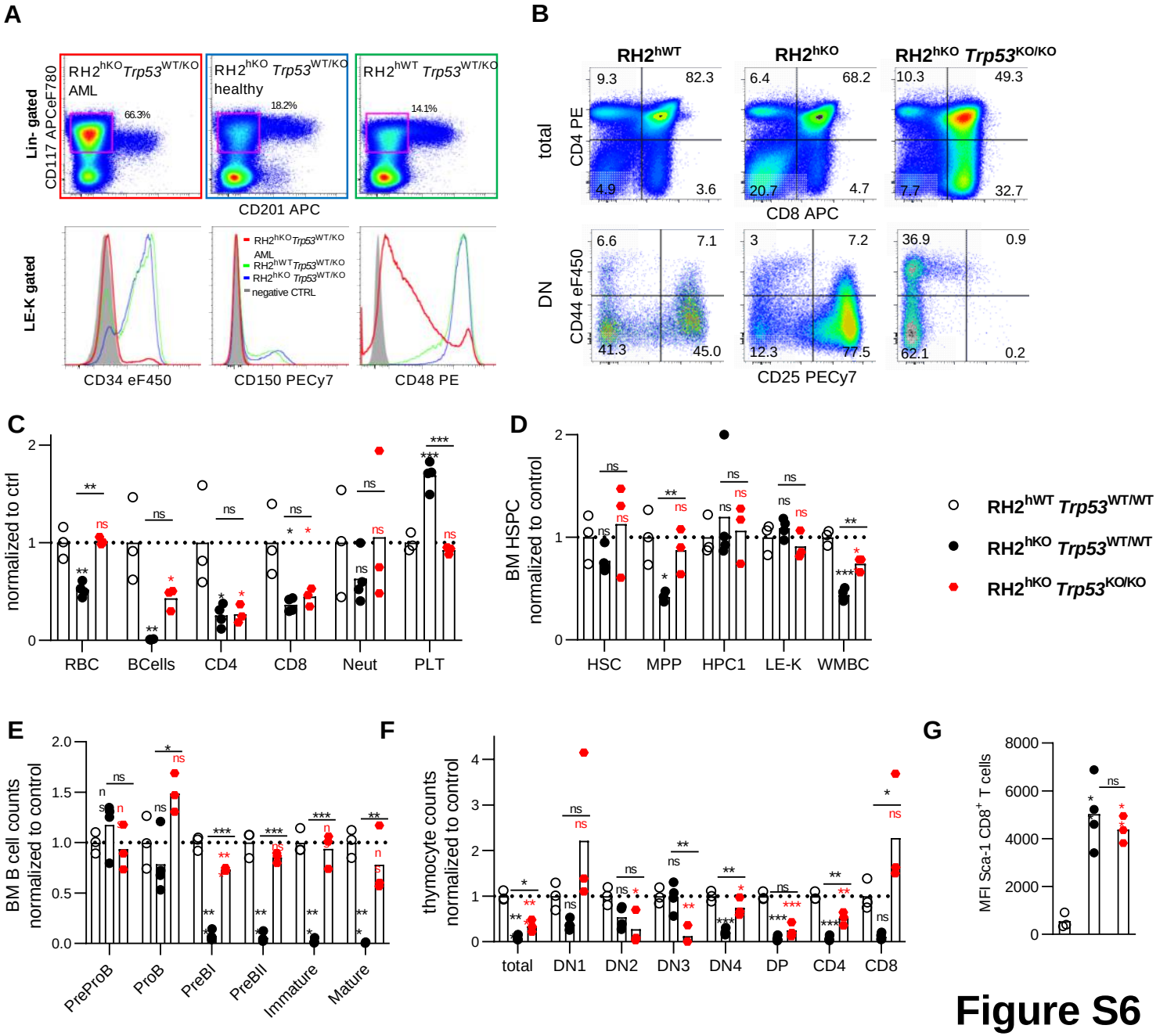
A
Lin- gated
CD117 APCeF780
RH2hKO Trp53WT/KO
AML
66.3%
RH2hKO Trp53WT/KO
healthy
18.2%
RH2hWT Trp53WT/KO
14.1%
CD201 APC
LE-K gated
RH2hKO Trp53WT/KO
AML
RH2hWT Trp53WT/KO
RH2hKO Trp53WT/KO
negative CTRL
CD34 eF450
CD150 PECy7
CD48 PE
B
RH2hWT
RH2hKO
RH2hKO Trp53KO/KO
total
CD4 PE
9.3
82.3
4.9
3.6
6.4
68.2
20.7
4.7
10.3
49.3
7.7
32.7
CD8 APC
DN
CD44 eF450
6.6
7.1
41.3
45.0
3
7.2
12.3
77.5
36.9
0.9
62.1
0.2
CD25 PECy7
C
PB counts [n/ml] normalized to ctrl
RBC
BCells
CD4
CD8
Neut
PLT
D
BM HSPC normalized to control
HSC
MPP
HPC1
LE-K
WMBC
RH2hWT Trp53WT/WT
RH2hKO Trp53WT/WT
RH2hKO Trp53KO/KO
E
BM B cell counts normalized to control
PreProB
ProB
PreBI
PreBII
Immature
Mature
F
thymocyte counts normalized to control
total
DN1
DN2
DN3
DN4
DP
CD4
CD8
G
MFI Sca-1 CD8+ T cells

Figure S6

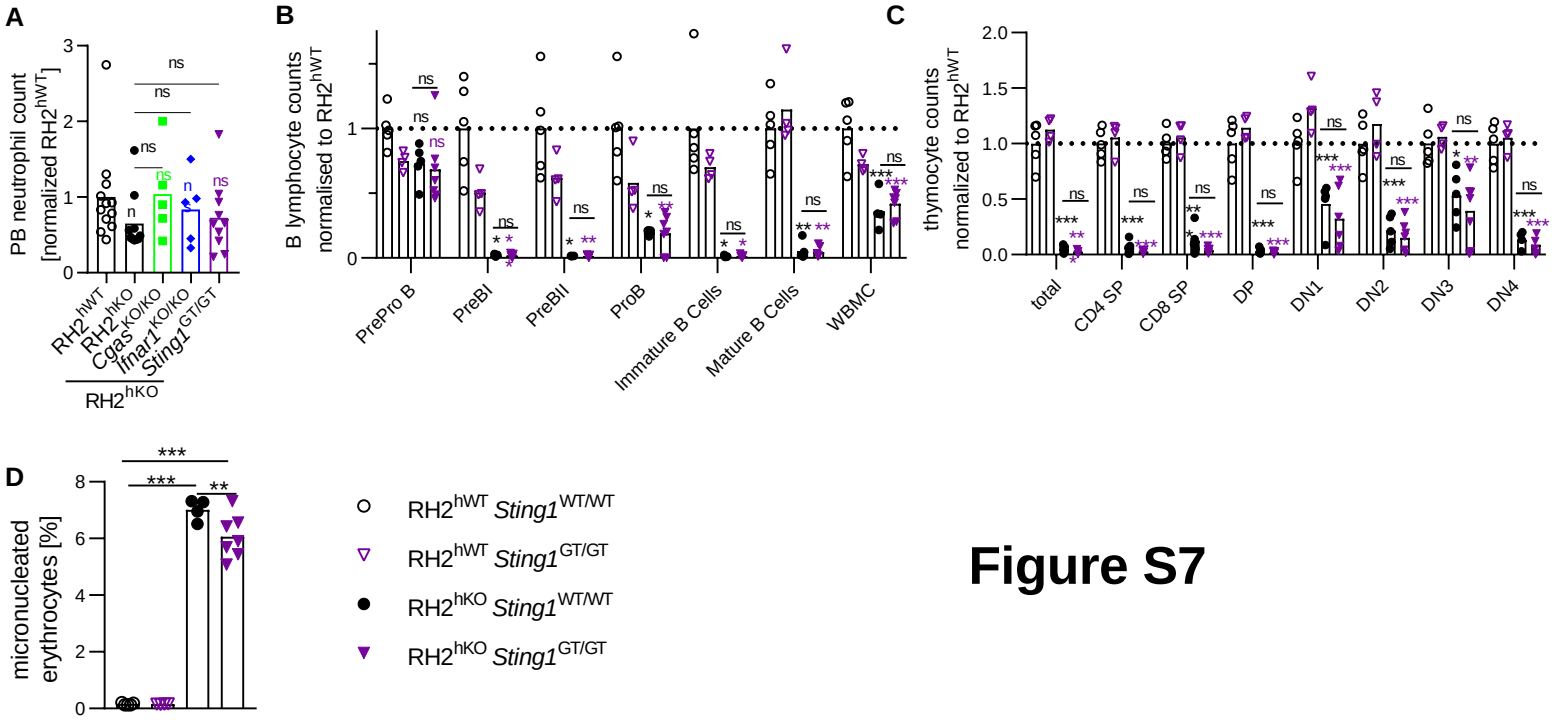
A
PB neutrophil count [normalized RH2hWT]
RH2hWT
RH2hKO
Cgas KO/KO
Ifnar1 KO/KO
Sting1 GT/GT
RH2hKO
B
B lymphocyte counts normalised to RH2hWT
PrePro B
PreBI
PreBII
ProB
Immature B Cells
Mature B Cells
WBMC
C
thymocyte counts normalized to RH2hWT
total
CD4 SP
CD8 SP
DP
DN1
DN2
DN3
DN4
D
micronucleated erythrocytes [%]
RH2hWT Sting1WT/WT
RH2hWT Sting1GT/GT
RH2hKO Sting1WT/WT
RH2hKO Sting1GT/GT

Figure S7

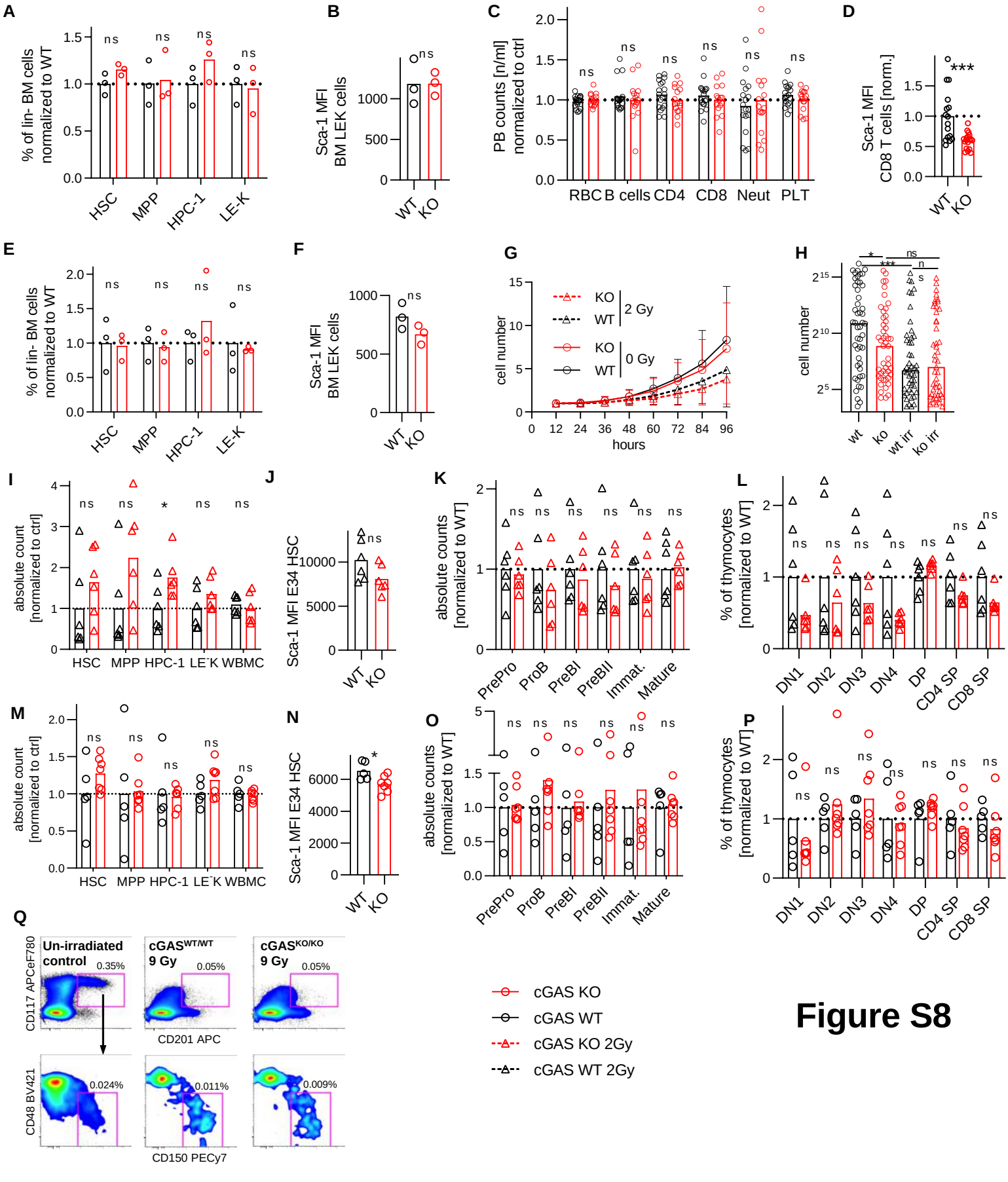
A
% of lin- BM cells normalized to WT
HSC
MPP
HPC-1
LE-K
B
Sca-1 MFI BM LEK cells
WT
KO
C
PB counts [n/ml] normalized to ctrl
RBC
B cells
CD4
CD8
Neut
PLT
D
Sca-1 MFI CD8 T cells [norm.]
E
F
G
cell number
hours
KO
WT
2 Gy
0 Gy
H
wt
ko
wt irr
ko irr
I
absolute count [normalized to ctrl]
WBMC
J
Sca-1 MFI E34 HSC
K
absolute counts [normalized to WT]
PrePro
ProB
PreBI
PreBII
Immat.
Mature
L
% of thymocytes [normalized to WT]
DN1
DN2
DN3
DN4
DP
CD4 SP
CD8 SP
M
N
O
P
Q
Un-irradiated control
cGAS WT/WT 9 Gy
cGAS KO/KO 9 Gy
0.35%
0.05%
0.05%
CD117 APCeF780
CD201 APC
CD48 BV421
CD150 PECy7
0.024%
0.011%
0.009%
cGAS KO
cGAS WT
cGAS KO 2Gy
cGAS WT 2Gy
Figure S8